C.R.N.

CRN/HE 84-01

MEASUREMENT OF Ξ DECAY PROPERTIES IN THE CERN SPS HYPERON BEAM

Bristol[1]-Geneva[2]-Heidelberg[3]-Orsay[4]-Rutherford[5]-Strasbourg[6] Collaboration

M.Bourquin[2], R.M.Brown[5], J.C.Chollet[4], A.Degre[6], D.Froidevaux[4], J.-M.Gaillard[4], C.N.P Gee[5], J.-P.Gerber[6], W.M.Gibson[1], P.Igo-Kemenes[3], P.W.Jeffreys[1], M.Jung[6], B.Merkel[4], R.Morand[6], H.Plothow-Besch[4], J.-P.Repellin[4], J.-L.Riester[6], B.J.Saunders[5], G.Sauvage[4], B.Schiby[6], H.W.Siebert[3], V.J.Smith[1], K.-P.Streit[3], R.Strub[6], S.N.Tovey[6] and J.J.Thresher[5].

centre de recherches nucléaires de Strasbourg

Institut National de Physique Nucléaire et de Physique des Particules

Université Louis Pasteur de Strasbourg

67037 STRASBOURG CEDEX FRANCE

MEASUREMENT OF Ω^- DECAY PROPERTIES IN THE CERN SPS HYPERON BEAM

Bristol[1]–Geneva[2]–Heidelberg[3]–Orsay[4]–Rutherford[5]–Strasbourg[6] Collaboration

M. Bourquin[2], R.M. Brown[5], J.C. Chollet[4], A. Degré[6], D. Froidevaux [2]–M. Gaillard[4], C.N.P. Gee[5], J.–P. Gerber[6], W.M. Gibson[1], P. Igo-Kemenes[3], P.W. Jeffreys[1], M. Jung[6], B. Merkel[4], R. Morand[6], H. Plothow-Besch[4], J.–P. Repellin[4], J.–L. Rieste[6], B.J. Saunders[5], G. Sauvage[4], B. Schiby[6], H.W. Siebert[3], V.J. Smith[1], K.–P. Streit[3], R. Strub[6], S.N. Tovey[7,6*] and J.J. Thresher[5].

(Submitted to Nuclear Physics)

1 H.H. Wills Physics Laboratory, University of Bristol, England.
2 University of Geneva, Switzerland.
3 Physikalisches Institut, Universität Heidelberg, Federal Republic of Germany**.
4 Laboratoire de l'Accélérateur Linéaire, Orsay, France.
5 Rutherford Appleton Laboratory, Didcot, England.
6 Division des Hautes Energies, CRN et Université Louis Pasteur, Strasbourg, France.
7 University of Melbourne, Australia.

* CERN Scientific Associate.
** Work supported by the Bundesministerium für Forschung und Technologie, Federal Republic of Germany.

ABSTRACT

In an experiment in the CERN SPS charged hyperon beam, a sample of 16,000 Ω^- decays was collected at an Ω^- momentum of 131 GeV/c. The Ω^- lifetime, the branching ratios and decay asymmetry parameters for the main decay modes were measured, giving:

$$\tau_{\Omega^-} = (0.823 \pm 0.015) \times 10^{-10}\,\mathrm{s}$$

$$\Gamma(\Omega^- \to \Lambda K^-)/\Gamma(\Omega^- \to \mathrm{all}) = 0.675 \pm 0.008, \qquad \alpha(\Omega^- \to \Lambda K^-) = -0.025 \pm 0.028$$
$$\Gamma(\Omega^- \to \Xi^0\pi^-)/\Gamma(\Omega^- \to \mathrm{all}) = 0.236 \pm 0.008, \qquad \alpha(\Omega^- \to \Xi^0\pi^-) = 0.09 \pm 0.14$$
$$\Gamma(\Omega^- \to \Xi^-\pi^0)/\Gamma(\Omega^- \to \mathrm{all}) = 0.089 \pm 0.005, \qquad \alpha(\Omega^- \to \Xi^-\pi^0) = 0.05 \pm 0.21$$

For the rare decay modes, the following results for the branching ratios were obtained:

$$\Gamma(\Omega^- \to \Xi^0 e^- \bar{\nu})/\Gamma(\Omega^- \to \mathrm{all}) = (0.56 \pm 0.28) \times 10^{-2}$$
$$\Gamma(\Omega^- \to \Xi^-\pi^+\pi^-)/(\Gamma(\Omega \to \mathrm{all}) = (3.7^{+3.6}_{-1.1}) \times 10^{-4}$$
$$\Gamma(\Omega^- \to \Xi^-\gamma)/(\Gamma(\Omega^- \to \mathrm{all}) < 2.2 \times 10^{-3} \text{ at the 90\% confidence level}$$
$$\Gamma(\Omega^- \to \Lambda\pi^-)/(\Gamma(\Omega^- \to \mathrm{all}) < 1.9 \times 10^{-4} \text{ at the 90\% confidence level.}$$

A sample of 32,000 Ξ^- decays collected under the same experimental conditions gave a new measurement of the Ξ^- lifetime:

$$\tau_{\Xi^-} = (1.652 \pm 0.051) \times 10^{-10}\,\mathrm{s}\ .$$

Combining the measurements of the present experiment with those obtained in a previous experiment in the SPS hyperon beam gives:

$$\tau_{\Omega^-} = (0.823 \pm 0.013) \times 10^{-10}\,\mathrm{s}$$

$$\Gamma(\Omega^- \to \Lambda K^-)/\Gamma(\Omega^- \to \mathrm{all}) = 0.678 \pm 0.007$$
$$\Gamma(\Omega^- \to \Xi^0\pi^-)/\Gamma(\Omega^- \to \mathrm{all}) = 0.236 \pm 0.007$$
$$\Gamma(\Omega^- \to \Xi^-\pi^0)/\Gamma(\Omega^- \to \mathrm{all}) = 0.086 \pm 0.004$$
$$\Gamma(\Omega^- \to \Xi^-\pi^+\pi^-)/\Gamma(\Omega^- \to \mathrm{all}) = (4.3^{+3.4}_{-1.3}) \times 10^{-4}.$$

The experimental results are compared with theoretical calculations.

1. INTRODUCTION

The first operation of the CERN SPS hyperon beam established the existence of a significant flux of Ω^-. Measurements of the Ω^- lifetime and branching ratios based on about 3000 decays have already been published [1,2]. Following the upgrading of the SPS external proton beam from 210 GeV/c to 240 GeV/c a new measurement has been performed with the hyperon beam momentum increased from 115 GeV/c to 131 GeV/c. The decay loss over the 12 *m* between the production target and the decay region was smaller by a factor of 2.4 at the higher momentum. In this article we report results on a new data sample of about 16,000 Ω^- decays.

We have measured the Ω^- branching ratios in the decay chains

(1) $\Omega^- \to \Lambda K^-$, $\Lambda \to p\pi^-$
(2) $\Omega^- \to \Xi^0\pi^-$, $\Xi^0 \to \Lambda\pi^0$, $\Lambda \to p\pi^-$, $\pi^0 \to \gamma\gamma$
(3) $\Omega^- \to \Xi^-\pi^0$, $\Xi^- \to \Lambda\pi^-$, $\Lambda \to p\pi^-$, $\pi^0 \to \gamma\gamma$
(4) $\Omega^- \to \Xi^0 e^- \bar{\nu}$, $\Xi^0 \to \Lambda\pi^0$, $\Lambda \to p\pi^-$, $\pi^0 \to \gamma\gamma$
(5) $\Omega^- \to \Xi^-\pi^+\pi^-$, $\Xi^- \to \Lambda\pi^-$, $\Lambda \to p\pi^-$,

and the decay asymmetry parameters for the modes (1), (2), and (3). Upper limits have been placed on the branching ratios for the decay modes

(6) $\Omega^- \to \Xi^-\gamma$, $\Xi^- \to \Lambda\pi^-$, $\Lambda \to p\pi^-$
(7) $\Omega^- \to \Lambda\pi^-$, $\Lambda \to p\pi^-$.

The Ω^- lifetime was obtained from the most abundant decay channel $\Omega^- \to \Lambda K^-$. We have also measured the Ξ^- lifetime from a sample of 32,000 $\Xi^- \to \Lambda\pi^-$ decays.

In section 2 of this paper we describe the apparatus and the trigger. The results on the main decay modes (1) to (3) are presented in section 3 and the rare decay modes in section 4. The comparison with theoretical calculations and the conclusions are given in section 5.

2. APPARATUS AND TRIGGER

2.1 Hyperon beam and experimental apparatus

The hyperon beam consisted of a magnetic channel and associated detection apparatus [3]. The magnetic channel comprised three bending magnets M1, M2,and M3, and two superconducting quadrupoles, Q1 and Q2 (see fig. 1). The hyperons were produced by the 240 GeV/c proton beam which struck a 32 cm BeO target located between the poles of M1. The magnetic channel, which had a momentum acceptance of 10% FWHM, selected negative particles with a mean momentum of 131 GeV/c, produced at an average angle of 2 mrad with respect to the proton beam. At the exit of the magnetic channel a DISC Čerenkov counter was used to trigger on Ω^- particles. The direction of the beam particles was measured with an accuracy of ± 0.07 mrad (r.m.s.), by five multiwire proportional chambers (beam chambers), located upstream and downstream of the DISC. The momentum of the beam particles was determined to better than 1% using a relation given by the beam optics, between horizontal angle and momentum [3].

The experimental apparatus is shown in fig. 2. The charged decay particles were analysed in a magnetic spectrometer which comprised a magnet with a bending power of 2.4 T·*m* and two sets of

drift chambers to measure the coordinates upstream (DC0–DC4) and downstream (DC5–DC8) of the magnet. The momentum resolution was $\delta p = \pm 1.5$ GeV/c at 100 GeV/c. The solid angle subtended by the magnet aperture and the drift chambers accepted all charged particles from $\Omega^- \rightarrow \Lambda K^-$, $\Lambda \rightarrow p\pi^-$ decays occurring in the 11.5 m long decay region upstream of the first drift chamber (DC1).

A lead-glass array [4] was used to measure the energy of γ-rays produced in Ω^- decay chains. A sandwich of two MWPCs and two 8 mm sheets of lead, placed immediately in front of the lead-glass array (see fig. 2), was used to locate γ-ray impact points for the decay channels (4) and (6). The efficiency and the accuracy of the γ-ray detection and π^0 reconstruction were measured as a function of the π^0 momentum using $\Sigma^+ \rightarrow p\pi^0$ decays obtained by retuning the hyperon beam for positive polarity at 100 GeV/c. For the study of the semi-leptonic decay channel $\Omega^- \rightarrow \Xi^0 e^- \bar{\nu}$, the electron identification was obtained by combining the information of the lead-glass array with that of the transition radiation detector [4] also shown in fig. 2, providing a total rejection of 20,000:1 against hadrons.

The main changes to the apparatus from that described in ref. [3] were that an additional drift chamber (DC0) was used to improve the track reconstruction in the beam region, and the lithium radiator of the first transition radiation detector was removed to reduce the probability of unwanted γ-ray conversions. The Čerenkov counter downstream of the magnet was not used in the analysis of the Ω^- decays.

2.2 Trigger and data collection

The trigger required an incident Ω^- by a coincidence between the beam telescope and the DISC together with the decay $\Lambda \rightarrow p\pi^-$ which was defined by a coincidence between the multiplicity counter and the proton counter.

For the beam telescope a $T0 \cdot T1 \cdot T2 \cdot \overline{A1} \cdot \overline{A2}$ coincidence was required, where T0, T1, T2 were the beam counters and A1, A2 the beam halo counters. The Ω^- were selected by the DISC. To obtain a high trigger efficiency, the DISC was equipped with a special profiled diaphragm [3] and at least 7 out of 8 phototubes were required to give a signal. (The detection efficiency thus obtained was 95% for Ω^- passing right through the DISC). To select events where the $\Lambda \rightarrow p\pi^-$ decay occurred before the first drift chamber we required a signal of more than one charged particle in the multiplicity counter in coincidence with a signal from the proton counter, which was located downstream of the spectrometer magnet and intercepted all protons from $\Lambda \rightarrow p\pi^-$ decays, but could not be reached by negative decay particles or beam particles. This decay trigger accepted 44% of all those Ω^- which triggered the DISC and decayed in the $\Omega^- \rightarrow \Lambda K^-$ mode.

The trigger rate was about 22 per 10^6 beam particles, in a beam spill of one second duration. A microprocessor [5] reduced this rate by a factor of 2 by rejecting high-multiplicity events using information from the beam chambers. Even so, the trigger rate was more than one order of magnitude greater than the genuine Ω^- counting rate. The background triggers were mainly due to multiparticle events and to $\Xi^- \rightarrow \Lambda\pi^-$, $\Lambda \rightarrow p\pi^-$ decay chains, which occurred before or inside the DISC and managed to fire seven of the eight DISC phototubes and also fulfilled the multiplicity and proton requirements. A total of 1.6×10^6 triggers were collected in 6 weeks.

At regular intervals, the DISC pressure was set to detect Ξ^- and triggers were taken in otherwise unchanged conditions. The $\Xi^- \rightarrow \Lambda\pi^-$ events, which have a decay topology similar to $\Omega^- \rightarrow \Lambda K^-$ decays, were used to monitor the performance of the apparatus. They were processed

immediately to check the efficiency of the data taking. Later in the course of the analysis, they were used to determine the parameters of the Monte Carlo simulation of the experiment and they also provided a measurement of the Ξ^- lifetime.

The correct DISC pressure setting for the Ω^- trigger was deduced from the relative positions of the Ξ^-, Σ^-, and π^- peaks in the pressure curve. The positions of these peaks were checked regularly during data taking.

Other auxiliary runs were performed at regular intervals during the data taking to monitor the performance of the electron and γ-ray detectors. The gain settings of the phototubes in the lead-glass array were checked in special runs with muons and the performance and the energy calibrations of both the transition radiation detector (XTRM) and the lead-glass array were checked with 6 GeV/c electrons obtained by retuning the hyperon beam as an electron beam [4].

3. Ω^- MAIN DECAY MODES

3.1 Event selection

3.1.1 Selection criteria common to all Ω^- decay channels

The first step in the analysis was to reduce the multiparticle background in the Ω^- data. Most of the genuine Ω^- decays and Ξ^- decays were expected to have a single charged particle at the exit of the DISC (the Ω^-/Ξ^- or a charged decay particle) with the $\Lambda \to p\pi^-$ decay occurring further downstream. The Ξ^- monitor sample was therefore used to determine an appropriate criterion for selecting Ω^- decays, based on the charged particle multiplicity at the exit of the DISC.

The $\Xi^- \to \Lambda\pi^-$ events were fully reconstructed by first requiring a $\Lambda \to p\pi^-$ decay, i.e. a positive and a negative track with an intersection situated within errors between $z = 2$ m and $z = 15.5$ m (see fig. 2) and having an effective mass $m_{p\pi^-}$ within ± 10 MeV/c^2 of the Λ mass. The width of the $m_{p\pi^-}$ distribution was 4 MeV/c^2 (FWHM). In addition to the Λ, a negative track was required, which, if interpreted as a π^- track, gave an effective mass $m_{\Lambda\pi^-}$ within ± 15 MeV/c^2 of the Ξ^- mass*). With these requirements the contamination in the Ξ^- sample was reduced to a negligible level.

A wire multiplicity was defined to be the sum of wires struck in the x and y planes of the third beam chamber which was situated just downstream of the DISC. With this definition the mean multiplicity for a single particle is approximately 5. A comparison of figs. 3a and 3b, which show the wire multiplicity distributions for beam triggers (mostly pions) and for the reconstructed Ξ^- sample, confirms that the multiparticle background in the Ξ^- sample is indeed small.

Figure 3c shows the same distribution for Ω^- triggers. The dominance of the multiparticle background is obvious. Events with a wire multiplicity larger than 12 were rejected, except in the search for the $\Omega^- \to \Xi^-\pi^+\pi^-$ decay mode. This cut reduced the multiparticle background in the Ω^- sample by a factor of 4. The loss due to this cut was 2.5% for Ξ^- decays and, because of the shorter lifetime, it was estimated to be 4% for Ω^- decays.

The presence of a $\Lambda \to p\pi^-$ decay was a common feature of all the Ω^- decay channels which were studied. Therefore, a reconstructed Λ, as defined above for the Ξ^- events, was required in all cases. The reconstructed Ω^- decay vertex, as defined later for each of the decay modes, had to be downstream of $z = 2$ m. For the decay $\Omega^- \to \Xi^0 e^- \bar{\nu}$, a cut at $z = 1.3$ m was applied instead. A reconstructed beam track was required in all cases, with the exception of the $\Omega^- \to \Lambda K^-$ and $\Xi^- \to \Lambda\pi^-$ events used for the lifetime determinations.

*) The width of the $m_{\Lambda\pi^-}$ distribution was 6 MeV/c^2 (FWHM).

3.1.2 Selection of $\Omega^- \to \Lambda K^-$ decays

An additional negative track was required which, if interpreted as a K^- track, gave with the reconstructed Λ an effective mass $m_{\Lambda K^-}$ within ± 60 MeV/c^2 of the Ω^- mass. The Ω^- decay point defined as the intersection of the K^- track and the reconstructed Λ track, had to be downstream of $z = 2$ m and within errors (typically $\delta z \approx \pm 0.2$ m), upstream of the Λ decay point. Furthermore, momentum balance was imposed by requiring the difference $\Delta\vec{p}$ between the measured Ω^- momentum and the sum of the Λ and K^- momenta, as measured with the spectrometer, to have components $|\Delta p_L| < 13$ GeV/c and $\Delta p_T < 0.23$ GeV/c. The widths of these distributions were $\delta p_L = 3.5$ GeV/c (r.m.s.) and $\delta p_T = 0.05$ GeV/c (r.m.s.). The $\Delta\vec{p}$ cut removed about 50% of the contamination due to $\Omega^- \to \Xi^0\pi^-$ events, in which momentum is carried off by a π^0.

Figure 4 shows the scatter plot $m_{\Lambda\pi^-}$ versus $m_{\Lambda K^-}$ of a partial sample (16%), where $m_{\Lambda\pi^-}$ is the effective mass obtained by interpreting the event as a $\Lambda\pi^-$ decay. In the case of events having more than one possible combination of decay tracks, the combination taken was that which was in closest agreement with the constraints $m_{p\pi^-} = m_\Lambda$, $|\Delta p_L| = 0$, $m_{\Lambda K^-} = m_\Omega$ and with geometrical matching between the track segments before and after the analysing magnet. This track combination was also used to determine $m_{\Lambda\pi^-}$. The figure shows a clear $\Omega^- \to \Lambda K^-$ signal together with a considerable background of $\Xi^- \to \Lambda\pi^-$ events. It was required that $m_{\Lambda\pi^-}$ be larger than 1.35 GeV/c^2, a cut which rejected practically all Ξ^-, but also 14% of the genuine $\Omega^- \to \Lambda K^-$ events. However, those $\Xi^- \to \Lambda\pi^-$ decays for which an additional spurious track was used to fake an $\Omega^- \to \Lambda K^-$ decay are not removed by the mass cut. To reject this type of background with the minimum loss of genuine $\Omega^- \to \Lambda K^-$ decays, the closest approximation to the $\Xi^- \to \Lambda\pi^-$ hypothesis was also defined for the constraints listed above in the case of events with several possible decay-track combinations. If the $\Xi^- \to \Lambda\pi^-$ hypothesis corresponded to a better approximation than the $\Omega^- \to \Lambda K^-$ hypothesis, the event was rejected. Figure 5 shows the scatter plot of the missing mass $MM(\Omega^- - \pi^-)$ versus $m_{\Lambda K^-}$ after these cuts, where $MM(\Omega^- - \pi^-)$ was obtained by interpreting the "K^-" track as a π^- track. The band around the Ξ^0 mass corresponds to $\Omega^- \to \Xi^0\pi^-$ background events. The distribution of $m_{\Lambda K^-}$ for the same sample is shown in fig. 6. The observed width is 6 MeV/c^2 (FWHM). Within $\pm$ 18 MeV/c^2 of the Ω^- mass the sample contains 12,082 events with an estimated background of 307 $\pm$ 37 $\Omega^- \to \Xi^0\pi^-$ events. The residual $\Xi^- \to \Lambda\pi^-$ background was estimated to be 60 $\pm$ 8 events by using the distributions of the $\Xi^- \to \Lambda\pi^-$ monitor sample.

3.1.3 Selection of $\Omega^- \to \Xi^0\pi^-$ decays

The Ω^- decay vertex, obtained by the intersection of a beam track and a negative particle track, had to be, within errors, upstream of the Λ vertex. Figure 7 shows the scatter plot of the effective mass $m_{\Lambda\pi^-}$ versus the missing mass $MM(\Omega^- - \pi^-)$, for a partial sample (16%). For events having more than one possible decay track combination, the track combination chosen for the calculation of $MM(\Omega^- - \pi^-)$ was the one which was in closest agreement with the constraints $m_{p\pi^-} = m_\Lambda$, $MM(\Omega^- - \pi^-) = m_{\Xi^0}$ and with geometrical matching between the track segments before and after the analysing magnet. For the calculation of $m_{\Lambda\pi^-}$, we chose the track combination which was in closest agreement with the $\Xi^- \to \Lambda\pi^-$ hypothesis. The curve drawn on fig. 7 represents the kinematical boundaries of the $(\Lambda\pi^-\pi^0)$ final state for Ω^- decays. The plot shows a clear Ξ^0 signal and a considerable Ξ^- background. The Ξ^- contamination comes mostly from Ξ^- triggering the DISC and to a small extent from $\Omega^- \to \Xi^-\pi^0$ decays. The diagonal band on this plot contains

$\Omega^- \rightarrow \Lambda K^-$ events where the K^- is interpreted as a π^- *). To suppress the Ξ^- background, we required $MM(\Omega^- - \pi^-)$ to be within ± 100 MeV/c^2 of the Ξ^0 mass. This cut removed 98% of the Ξ^- decays. In the absence of measurement errors the $\Omega^- \rightarrow \Lambda K^-$ decays would have a longitudinal momentum balance $\Delta p_L = p_L^{\Omega^-} - p_L^{\Lambda} - p_L^{K^-} = 0$. In practice, the measured standard deviation on Δp_L is 3.5 GeV/c. To reject further this type of background we required $\Delta p_L > 7.2$ GeV/c. This cut removed 94% of the residual ΛK^- contamination but also 15% of the genuine $\Omega^- \rightarrow \Xi^0 \pi^-$ events. In addition we required the squared $(\Omega^- - \Lambda - \pi^-)$ missing mass, which should equal $m_{\gamma\gamma}^2$, to be within the range $-0.03 < MM^2(\Omega^- - \Lambda - \pi^-) < 0.06$ (GeV/c^2)^2. Figure 8 gives the scatter plot $m_{\Lambda\gamma}$ versus $MM(\Omega^- - \pi^-)$ for the resulting sample. The figure shows a Ξ^0 signal concentrated mainly inside the kinematic limits and a small residual Ξ^- background. The Ξ^0 and Ξ^- events outside the limits are multitrack events where the track combinations for $MM(\Omega^- - \pi^-)$ and $m_{\Lambda\pi^-}$ are different. To reduce further the Ξ^- background, we rejected events which gave a closer agreement with the $\Xi^- \rightarrow \Lambda\pi^-$ hypothesis than with the $\Xi^0\pi^-$ hypothesis. This selection removed all the Ξ^- from the sample except for a very small contribution in the (Ξ^0, Ξ^-) crossing region.

At this selection level the residual background consisted mainly of $\Omega^- \rightarrow \Lambda K^-$ decays, as shown by fig. 9 which gives $m_{\Lambda K^-}$ versus $MM(\Omega^- - \pi^-)$. Figure 10a is the $MM^2(\Omega^- - \Lambda - \pi^-)$ distribution for the same sample showing a clean peak centred at $m_{\pi^0}^2$. The $(\Omega^- - \pi^-)$ missing-mass distribution is shown in fig. 10b. The width of the Ξ^0 mass peak is 10 MeV/c^2 (FWHM) and there are 2013 events within ± 40 MeV/c^2 of the Ξ^0 mass and 1759 events within ± 20 MeV/c^2. The amount of residual background is discussed in subsection 3.2, where information from the γ-ray detectors is also used.

3.1.4 Selection of $\Omega^- \rightarrow \Xi^-\pi^0$ decays

The candidates for this decay channel were selected by the following requirements, in addition to a Λ as defined previously. There was an additional negative track which, if interpreted as a π^-, gave an effective mass $m_{\Lambda\pi^-}$ within ± 20 MeV/c^2 of the Ξ^- mass. Within errors, both the Ξ^- and Λ decay vertices were located within the range $2.0 < z < 13.5$ m with the Λ vertex downstream of the Ξ^- vertex. The Ω^- vertex, i.e. the intersection of the reconstructed Ξ^- track with the beam track, was within errors upstream of the Ξ^- vertex.

The π^0 momentum was defined as the difference $\Delta\vec{p}$ between the beam momentum and the Ξ^- momentum. In fig. 11 we show a scatter plot of MM_X^2, the square of the $(\Omega^- - \Xi^-)$ missing mass, versus the longitudinal component Δp_L for a fraction (16%) of the selected events. The full curve drawn on the figure corresponds to $\Xi^- \rightarrow \Lambda\pi^-$ events, interpreted as $\Omega^- \rightarrow \Xi^- + X$, with a reconstructed $\Delta p_T = 0$. For $\Delta p_T > 0$, the $\Xi^- \rightarrow \Lambda\pi^-$ events lie below this curve. The events situated near the boundary curve with values of $|\Delta p_L| \leq 10$ GeV/c are due to contamination from Ξ^- produced in the target with a momentum close to the average beam momentum. The events close to the upper part of the curve with $\Delta p_L \simeq 30$ GeV/c correspond to Ξ^- with an average velocity equal to the Ω^- velocity for which the DISC was tuned. Such a low momentum Ξ^- background was expected from $\Omega^- \rightarrow \Xi^-\pi^0$ decays in the magnetic channel. To select the $\Omega^- \rightarrow \Xi^-\pi^0$ events, we required:

$$\Delta p_L > |0.12 + MM_X^2/(m_\Omega^2 - m_\Xi^2)| \, p_{beam} \, .$$

This is the straight part of the dashed line in fig. 11. This cut removed most of the Ξ^- contamination at low $|\Delta p_L|$ and a large fraction of the low momentum Ξ^-. We further reduced the Ξ^- background

*) To a very good approximation, $[MM(\Omega^- - \pi^-)]^2 + m_{\pi^-}^2 = m_\Omega^2 + m_\Lambda^2 + m_\pi^2 - m_K^2$ for $\Omega^- \rightarrow \Lambda K^-$ decays.

by requiring $\Delta p_T > 0.15$ GeV/c. This cut corresponds to the curved part of the dashed line. The two cuts together removed 98% of the total background but also 40% of genuine $\Omega^- \to \Xi^-\pi^0$ events. Figure 12 shows the total $\Omega^- \to \Xi^-\pi^0$ sample after these cuts. There is a clear signal in the π^0 mass region. In fig. 13 we show the distribution of MM_X^2. The final sample was obtained by requiring $-0.016 < MM_X^2 < 0.052\,(GeV/c^2)^2$ and contains 862 events.

3.2 $\Omega^- \to \Xi^0\pi^-$ and $\Omega^- \to \Xi^-\pi^0$ signal and background determinations

3.2.1 Method

To evaluate the signals and the backgrounds of the $\Xi\pi$ decay modes, we used the fact that both channels have among their decay products a π^0 which decays into two γ-rays. Therefore, requiring a signal in the lead-glass array reduced the background of events which did not contain a γ-ray. We used a simple algorithm, which ensured a high γ efficiency and minimized possible biases, giving a background rejection factor of 3.

Let N_1 be the number of events in a $\Omega^- \to \Xi\pi$ sample of which N_1' have an accepted lead-glass signal; then the $\Xi\pi$ signal S_1 and the background B_1 are solutions of the two equations

$$N_1 = S_1 + B_1$$

$$N_1' = \varepsilon S_1 + r B_1 \ ,$$

where $\varepsilon(r)$ is the fraction of signal (background) events which were accepted by the lead-glass requirement.

The same relations hold for the events situated on either side of the signal region and we can write:

$$N_2 = S_2 + B_2$$

$$N_2' = \varepsilon S_2 + r B_2 \ ,$$

where N_2 is the sum of the events on either side of the signal interval, N_2' the sum of the events situated in the same regions but with a detected lead-glass signal, S_2 the residual signal, B_2 the background, ε and r the same variables as before. Thus, we have a set of four independent equations with 6 unknowns. To solve the system two additional constraints are needed. For each decay mode the additional information required to solve this set of equations is presented below.

3.2.2 $\Omega^- \to \Xi^0\pi^-$ signal and background determination

For this channel the quantity r was estimated using the $(\Omega^- - \pi^-)$ missing-mass distribution of fig. 10b, where the regions beyond ± 50 MeV/c^2 from the Ξ^0 mass are expected to contain only background events. The result obtained was:

$$r = 0.36 \pm 0.04 \ .$$

The second constraint was derived from a relation between B_1 and B_2. Since 95% of the background in the data sample was due to $\Omega^- \to \Lambda K^-$ decays, we used the Monte Carlo simulation program described in subsection 3.3 to generate such decays. These events were then processed

through the complete $\Omega^- \to \Xi^0\pi^-$ analysis program. The distribution of the $(\Omega^- - \pi^-)$ missing mass thus obtained was linear within ± 40 MeV/c^2 of the Ξ^0 mass.

For the data sample, N_1 was the number of events within ± 20 MeV/c^2 of the Ξ^0 mass (see fig. 10b) and N_2 the sum of the number of events in the two 20 MeV/c^2 intervals on either side of this mass range. On the basis of the Monte Carlo simulation we found that the $\Omega^- \to \Lambda K^-$ background contributed equally to B_1 and B_2. The very small residual Ξ^- background, entirely contained in the (Ξ^0, Ξ^-) crossing region of fig. 8, was estimated to be 23 ± 5 events by assuming a linear dependence of the genuine $\Omega^- \to \Xi^0\pi^-$ signal on $m_{\Lambda\pi^-}$, within ± 50 MeV/c^2 of the Ξ^- mass. The whole Ξ^- background contribution is within ± 20 MeV/c^2 of the Ξ^0 mass. Thus we have $B_1 = B_2 + 23$.

From the experimental numbers, $N_1 = 1759$, $N_1' = 1357$, $N_2 = 254$, and $N_2' = 126$, we obtained:

$$\varepsilon = 0.825 \pm 0.014 \ ,$$

$$S_1 = 1556 \pm 52 \ , \qquad B_1 = 203 \pm 28 \ ,$$

$$S_2 = \ \ 74 \pm 24 \ , \qquad B_2 = 180 \pm 28 \ .$$

Thus the total $\Omega^- \to \Xi^0\pi^-$ signal within ± 40 MeV/c^2 of the Ξ^0 mass is $S = S_1 + S_2 = 1630 \pm 65$ events and the background amounts to 383 ± 54 events. The errors include the statistical errors on the sample size and the uncertainties connected with the estimation of r.

The efficiency ε is an average over the π^0 momentum spectrum. Figure 14 shows the variation of ε as a function of the missing longitudinal momentum Δp_L. The decrease of ε for small Δp_L is due to the geometrical acceptance. This variation of ε could possibly introduce a bias in the signal determination. Therefore as a check we divided the Δp_L range into three independent intervals and, computing the signal for each of them, we found a total of 1627 events in good agreement with the number given above.

3.2.3 $\Omega^- \to \Xi^-\pi^0$ signal and background determination

The determination of the signal for this channel was more difficult than for $\Omega^- \to \Xi^0\pi^-$ because the background was larger and arose from more than one source. Therefore a linear interpolation from the side regions into the $m^2_{\pi^0}$ peak (fig. 13) was not appropriate. The gamma-detection efficiency ε was obtained as a function of the missing longitudinal momentum by correcting the efficiency curve measured for the decay $\Omega^- \to \Xi^0\pi^-$ (fig. 14) for the difference in geometrical acceptance between the two decay channels. Figure 14 shows also the resulting curve. The mean value over the accepted Δp_L range was

$$\varepsilon = 0.939 \pm 0.016 \ .$$

The efficiency is larger than in the $\Omega^- \to \Xi^0\pi^-$ case because the average π^0 momentum of the selected events is larger (see figs. 17a and 18). The fraction r of the background events which gave a spurious γ-ray signal was estimated for different Δp_L intervals by selecting events on either side of the π^0 signal, i.e. $MM_X^2 > 0.086\ (\mathrm{GeV/c^2})^2$ or $MM_X^2 < -0.05\ (\mathrm{GeV/c^2})^2$.

It was found to be constant within errors over the full Δp_L range spanned by the missing π^0. The mean value was

$$r = 0.28 \pm 0.05 \ .$$

Using the values of ε and of r, the signal and the background were derived from the two equations

$$N_1 = S_1 + B_1$$

$$N_1' = \varepsilon S_1 + r B_1 \ .$$

From the experimental numbers $N_1 = 862$, $N_1' = 646$, we obtained

$$S_1 = 614 \pm 37 \ , \qquad B_1 = 248 \pm 33 \ .$$

The errors include the statistical errors on the sample size and the uncertainties on r and ε.

3.3 Monte Carlo Simulation

In order to obtain lifetimes, branching ratios, and asymmetries from the data, it was necessary to correct for the geometrical acceptance of the apparatus, the reconstruction efficiencies, and the effects of kinematic cuts. These corrections have been determined from a detailed Monte Carlo (MC) simulation of the experiment. The MC events were analysed with the same set of programs as were used for the data. The parameters describing the apparatus were chosen so that the MC accurately reproduced the decay distributions for the $\Xi^- \to \Lambda\pi^-$ event sample described in subsection 3.1.1. The Ω^- decays were then simulated using the same parameters.

3.3.1 Description of the Monte Carlo model

The incident hyperon trajectories were generated using the known beam optics [3] and the observed distributions in the beam chambers. As the hyperons traversed the apparatus they underwent sequential decays. In cases where the first decay occurred before the end of the DISC, the event was weighted with a detection efficiency which depended on the distance the hyperon travelled through the DISC before decaying.

The charged decay products were propagated through the spectrometer magnet using the measured field map. They underwent appropriate multiple scattering and, in the case of electrons, also emitted bremsstrahlung. There was 7% of a radiation length between the DISC exit and the magnet entrance including 2% in the lithium radiator. Coordinate measurements in the chambers were obtained from the tracks, using the appropriate resolution functions and detection efficiencies. In the case of the beam chambers the smearing was applied directly to the spatial coordinates, whereas, for the drift chambers, simulated drift times were created with the measured timing resolution functions.

Over most of the sensitive area of the drift chambers the accuracy and efficiency were uniform. However, there was a rapid variation of these two parameters in a small region close to the beam axis, caused by space-charge effects. A fraction of the protons emitted by the Λ in the decay chain

passed through the beam region of the drift chambers in front of the magnet (14% for $\Omega^- \to \Lambda K^-$ decays and 40% for Ξ^- decays). A detailed study of protons from the sequential decay $\Xi^- \to \Lambda\pi^-$, $\Lambda \to p\pi^-$ was therefore conducted to ensure that the measurement accuracy and inefficiency were correctly reproduced by the MC. Figure 15 shows a comparison between distributions of R_p (the distance of the proton from the beam axis at $z = 15$ m) for the data and two sets of MC events. One MC distribution was generated neglecting the drift-chamber inefficiencies in the beam region; for the other these were taken into account. From the differences between the two MC curves it was estimated that 8% of the $\Xi^- \to \Lambda\pi^-$, $\Lambda \to p\pi^-$ decays were lost because of this effect. For the Ω^- decays this loss was much smaller.

3.3.2 Comparisons between data and MC distributions

A series of comparisons was made between the data and the MC distributions to check that the simulation was adequate. In the following we present the results of some of the more important tests, and we discuss some special features in the MC program used for the $\Omega^- \to \Xi^-\pi^0$ decay.

$\Omega^- \to \Lambda K^-$ decay

The data sample used for the comparisons was that defined in subsection 3.1.2. The effective mass distribution is particularly sensitive to the chamber resolutions. Figure 6 shows the MC/data comparison of the (ΛK^-) effective mass. The data and MC distributions are in agreement apart from the tails which are more pronounced in the data. A large fraction of this excess is due to the $\Omega^- \to \Xi^0\pi^-$ background events, which give a flat effective mass distribution when interpreted as $\Omega^- \to \Lambda K^-$ (see fig. 5). The Λ momentum distribution is shown in fig. 16a and the distribution of the Λ angle with respect to the beam particle in fig. 16b. The data are adequately reproduced by the MC distributions.

$\Omega^- \to \Xi^0\pi^-$ decay

The $(\Xi^0\pi^-)$ data sample of 1759 events (including 203 ± 28 background events) was that defined in subsection 3.1.3. For the MC/data comparison the small $\Xi^- \to \Lambda\pi^-$ contamination was reduced to a negligible level by rejecting events with a $(\Lambda\pi^-)$ mass within ±15 MeV/c^2 of the Ξ^- mass. In addition, for the data sample, events outside the selected $(\Omega^- - \pi^-)$ missing-mass window were used to subtract statistically the residual background for all distributions. This sample was also used for the determination of the Ω^- lifetime and the asymmetry parameter in this decay mode. Figure 17a shows the MC/data comparison of the $(\Omega^- - \Lambda - \pi^-)$ missing longitudinal momentum distributions. The full histogram corresponds to the data sample after background subtraction, the dashed histogram to the background itself. The $\Omega^- \to \Lambda K^-$ contamination was expected at the lower end of the missing-momentum spectrum. The agreement between the full histogram and the MC distribution shows that the background subtraction was adequate. Figure 17b shows the MC/data comparison of the angle between the Ω^- and the π^-. The range spanned by this angle was larger than for any other decay. The good agreement of the MC and data distributions was a critical check of the geometrical input parameters.

$\Omega^- \to \Xi^-\pi^0$ decay

The MC simulation had to describe problems specific to this decay mode for Ω^- decaying inside the DISC. For instance it is only for this decay mode that an important amount of Čerenkov

light emitted by the charged decay particle can reach the DISC phototubes because the velocity of the Ξ^- is on an average equal to that of the Ω^- and the decay angle is small. Also due to the large angle between the π^0 and the Ω^-, 2.8% of the γ-rays converted in the mirror or in the flange of the DISC. These events were vetoed by the halo counter A2 (see fig. 1).

For the data sample, the background of 248 events (see subsection 3.2.3) was subtracted by using the events outside the $MM^2(\Omega^- \sim \Xi^-)$ window (fig. 13). The distributions of the missing longitudinal momentum are shown in fig. 18 for the data after background subtraction, for the background itself and for the MC events.

3.4 Ω^- and Ξ^- lifetimes

3.4.1 $\Omega^- \to \Lambda K^-$ decay

For the determination of the Ω^- lifetime, we did not use the beam-chamber information in order to avoid potential errors from a confusion of Ω^- and K^- tracks in the beam chambers. The momentum balance cuts were replaced by the requirement $|\vec{p}_\Lambda + \vec{p}_{K^-}| > 115$ GeV/c, which was almost as effective for the $(\Xi^0\pi^-)$ background rejection and made no use of the beam chambers. Furthermore, a more restrictive cut than described in subsection 3.1.2 was applied to the effective mass $m_{\Lambda\pi^-}$ by rejecting events where any combination of spectrometer tracks yielded $m_{\Lambda\pi^-} < 1.35$ GeV/c^2. The requirements on the effective mass $m_{\Lambda K^-}$ and on the vertex ordering were the same as for the branching-ratio sample. The distribution of the Ω^- decay points as obtained from the intersection of the K^- track and the reconstructed Λ track is shown in fig. 19. For $z > 2$ m, the sample contains 13,800 events. The difference between this sample and the branching-ratio sample is mainly due to the inefficiencies of the beam chambers and to the beam track reconstruction. The background of (330 ± 40) $\Omega^- \to \Xi^0\pi^-$ events in this sample was taken into account by adding to the MC events a corresponding amount of $\Omega^- \to \Xi^0\pi^-$ MC events which had survived the $\Omega^- \to \Lambda K^-$ selection. After cuts the MC sample contained 50,000 events, whose weights were calculated for each Ω^- lifetime assumed in the fitting procedure. Table 1 shows the results of the fits for different cuts in the z-coordinate along the beam, where the quoted errors are statistical only. The samples with an upstream fiducial cut at 2 m included events which decayed inside the DISC. For these samples it was therefore necessary to apply a correction for the variation of the DISC efficiency with the distance travelled by the Ω^- inside the DISC before decaying. There is an uncertainty of 7% in the mean number of photoelectrons used in the calculation which introduces an additional systematic uncertainty on the lifetime, $\delta\tau_{\Omega^-} = 0.008 \times 10^{-10}$ s. To avoid this uncertainty we therefore use the value obtained from the sample with $2.8 < z < 10$ m:

$$\tau_{\Omega^-} = (0.823 \pm 0.013) \times 10^{-10} \text{ s} .$$

The MC distribution of the decay points obtained for this value of τ_{Ω^-} is shown by the curve in fig. 19, which is in good agreement with the data distribution. The variation of χ^2 with τ_{Ω^-} in the fit for the chosen interval $2.8 < z < 10$ m is also shown in fig. 19. To check on possible background effects, we subtracted statistically the estimated amount of $\Omega^- \to \Xi^0\pi^-$ background from the data using the decay-point distribution of the events with $|m_{\Lambda K^-} - m_{\Omega^-}| > 25$ MeV/c^2. From the lifetime fit using the pure $\Omega^- \to \Lambda K^-$ MC sample we obtained $\tau_{\Omega^-} = (0.822 \pm 0.013) \times 10^{-10}$ s in the same decay region.

3.4.2 $\Omega^- \to \Xi\pi$ decays

The Ω^- lifetime has also been determined for the $\Omega^- \to \Xi\pi$ decay modes as a cross-check of the analysis procedures and the acceptance calculations.

The $\Omega^- \to \Xi^0\pi^-$ sample with the background subtracted was the same as for the MC/data comparison (see subsection 3.3.2). The Ω^- decay point was obtained from the intersection of the π^- track and the beam track. The reconstruction error was 0.18 m (r.m.s.), slightly smaller than for the $\Omega^- \to \Lambda K^-$ mode because of the larger decay angles. The resulting decay point distribution is shown in fig. 20a. For $z > 2$ m, the sample contained 1505 events. The results of the fits for different decay regions are given in Table 2. In the inverval $2.8 < z < 8$ m we obtained:

$$\tau_{\Omega^-} = (0.82 \pm 0.05) \times 10^{-10}\,\mathrm{s}\ ,$$

where the error is statistical only. The MC distribution corresponding to this result is given by the curve in fig. 20a; it shows good agreement with the data.

For the lifetime determination in the $\Omega^- \to \Xi^-\pi^0$ decay mode we used the branching-ratio sample (subsection 3.2.3), which contained 614 events after subtraction of 248 background events. The distribution of the Ω^- decay points obtained from the beam track and the reconstructed Ξ^- track is shown in fig. 20b. In the interval $2.8 < z < 8.4$ m the result of the fit was

$$\tau_{\Omega^-} = (0.92 \pm 0.07) \times 10^{-10}\,\mathrm{s}\ .$$

The agreement between the lifetime results for the $\Xi\pi$ decay modes and the ΛK^- decay mode gives further support to the validity of the MC calculations and the adequacy of the background treatment.

3.4.3 $\Xi^- \to \Lambda\pi^-$ decay

The data sample was collected in special runs distributed over the whole Ω^- data-taking period. After the selection described in subsection 3.1.1 the sample contained 41,200 events. The Ξ^- decay point was obtained from the intersection of the π^- track and the reconstructed Λ track, with an error of 0.20 m (r.m.s.) along the beam direction. As in the case of the decay $\Omega^- \to \Lambda K^-$, we thus avoided the use of the beam-chamber information for the lifetime determination. The resulting decay-point distribution is shown in fig. 21. Table 3 lists the results of the lifetime fits for different decay regions, based on a sample of 10^5 $\Xi^- \to \Lambda\pi^-$ MC events after cuts. We use the value obtained from the 31,817 events in the decay region $2.8 < z < 10$ m (as for $\Omega^- \to \Lambda K^-$),

$$\tau_{\Xi^-} = (1.652 \pm 0.033) \times 10^{-10}\,\mathrm{s}\ ,$$

where the error is statistical only. The MC distribution corresponding to this value is shown by the curve in fig. 21, which again is in good agreement with the data. The variation of χ^2 with τ_{Ξ^-} is also shown in fig. 21.

3.4.4 Systematic errors

The largest contribution to the systematic errors of the lifetime determinations arose from the uncertainties of the drift-chamber inefficiencies in the beam region (DC0-DC4), which resulted in systematic errors

$$\delta\tau_{\Omega^-} = 0.005 \times 10^{-10}\,\mathrm{s} \qquad \text{and} \qquad \delta\tau_{\Xi^-} = 0.037 \times 10^{-10}\,\mathrm{s}\ .$$

The absolute beam momentum was known with an accuracy of 0.5%, with resulting errors

$$\delta\tau_{\Omega^-} = 0.004 \times 10^{-10}\,\mathrm{s} \qquad \text{and} \qquad \delta\tau_{\Xi^-} = 0.008 \times 10^{-10}\,\mathrm{s}\ .$$

If the lifetime of the Λ, which is used in the MC calculation, is increased from the world average value [6], $\tau_\Lambda = 2.632 \times 10^{10}$ s, by the experimental error $\delta\tau_\Lambda = 0.020 \times 10^{-10}$ s, the measured lifetimes increase by

$$\delta\tau_{\Omega^-} = 0.002 \times 10^{-10}\,\mathrm{s} \qquad \text{and} \qquad \delta\tau_{\Xi^-} = 0.008 \times 10^{-10}\,\mathrm{s}\ .$$

The total systematic errors are

$$\delta\tau_{\Omega^-} = 0.007 \times 10^{-10}\,\mathrm{s} \qquad \text{and} \qquad \delta\tau_{\Xi^-} = 0.039 \times 10^{-10}\,\mathrm{s}$$

for the $\Omega^- \to \Lambda K^-$ and the $\Xi^- \to \Lambda\pi^-$ decays respectively.

These systematic errors have been added in quadrature to the statistical errors.

3.4.5 Comparison with earlier measurements

The result for the Ω^- lifetime

$$\tau_{\Omega^-} = (0.823 \pm 0.015) \times 10^{-10}\,\mathrm{s}$$

is in agreement with the earlier hyperon-beam result obtained from a sample six times smaller collected at 98 and 115 GeV/c,

$$\tau_{\Omega^-} = (0.822 \pm 0.028) \times 10^{-10}\,\mathrm{s}\ (\text{ref. [1]})$$

and with two bubble-chamber results, $\tau_{\Omega^-} = (0.80^{+0.16}_{-0.12}) \times 10^{-10}$ s (ref. [7]) and $\tau_{\Omega^-} = (0.75^{+0.14}_{-0.11}) \times 10^{-10}$ s (ref. [8]).

The result for the Ξ^- lifetime,

$$\tau_{\Xi^-} = (1.652 \pm 0.051) \times 10^{-10}\,\mathrm{s}\ ,$$

is in agreement with the earlier hyperon beam result obtained at 98 and 115 GeV/c from a sample of equal size $\tau_{\Xi^-} = (1.665 \pm 0.065) \times 10^{-10}$ s (ref. [1]) and with the average value from three other precise measurements in bubble chambers $\tau_{\Xi^-} = (1.617 \pm 0.028) \times 10^{-10}$ s (refs. [8-10]).

3.5 $\Omega^- \to \Lambda K^-$ and $\Omega^- \to \Xi\pi$ decay branching ratios

The numbers of events for each decay mode are given in Table 4, together with the relative acceptances obtained by MC calculation. From these numbers we obtained the ratios

$$R_1 = \Gamma(\Omega^- \to \Lambda K^-)/\Gamma(\Omega^- \to \Xi^0\pi^-) = 2.86 \pm 0.12$$

and

$$R_2 = \Gamma(\Omega^- \to \Xi^0\pi^-)/\Gamma(\Omega^- \to \Xi^-\pi^0) = 2.65 \pm 0.19 \ ,$$

where the errors are statistical only. For the calculation of the branching ratios we have assumed that the contributions of these 3 modes add up to 100% of the Ω^- decays.

Systematic errors in the acceptances are important only if they are different for the various decay modes; thus we have investigated the uncertainties on the ratios R_1 and R_2. The calculation of the DISC efficiency for Ω^- decays occurring inside the sensitive volume of the DISC introduces an uncertainty $\delta R_1/R_1 = \pm 0.4\%$, owing to the different Ω^- decay-point distributions for the final event samples. Uncertainties in the measurement of the efficiencies of the drift chambers (DC0-DC4) in the beam region give rise to $\delta R_1/R_1 = \pm 0.5\%$. Finally the uncertainties in the lifetimes of the particles contribute $\delta R_1/R_1 = \pm 1.5\%$, of which the major part is due to the error on the Ξ^0 lifetime. The total systematic error in the ratio of the acceptances for the ΛK^- and the $\Xi^0\pi^-$ decay modes is then $\delta R_1/R_1 = \pm 1.6\%$. The systematic error in the ratio of the $\Xi\pi$ acceptances arising from the same error sources is mostly due to the uncertainties in the lifetimes. We obtained $\delta R_2/R_2 = \pm 1.6\%$, and thus

$$R_1 = \Gamma(\Omega^- \to \Lambda K^-)/\Gamma(\Omega^- \to \Xi^0\pi^-) = 2.86 \pm 0.13$$

$$R_2 = \Gamma(\Omega^- \to \Xi^0\pi^-)/\Gamma(\Omega^- \to \Xi^-\pi^0) = 2.65 \pm 0.20$$

and the branching ratios listed in Table 4. The quoted errors include the estimated systematic uncertainties. Table 4 also contains the branching ratios obtained in the previous experiment [2]. The two sets of measurements are in good agreement.

3.6 Ω^- decay asymmetry parameters

The main Ω^- decay modes

$$\Omega^- \to \Lambda K^-$$
$$\Omega^- \to \Xi^0\pi^-$$
$$\Omega^- \to \Xi^-\pi^0$$

are the only observed examples of non-leptonic weak transitions between the $J^P = 3/2^+$ and $J^P = 1/2^+$ multiplets of SU(3).

These decays may occur via P and/or D amplitudes leading to the following expression for the α parameters:

$$\alpha = 2\,\mathrm{Re}(P^*D)/(|P|^2 + |D|^2) \ .$$

Thus α gives the amount of parity mixing for each decay mode.

As the mean production angle of the beam was close to zero (2 mrad), the Ω^- were not polarized. The α parameters were obtained from the angular distributions of the final baryon in the decay chains ($\Omega^- \to \Lambda K^-$, $\Lambda \to p\pi^-$), ($\Omega^- \to \Xi^0\pi^-$, $\Xi^0 \to \Lambda\pi^0$), and ($\Omega^- \to \Xi^-\pi^0$, $\Xi^- \to \Lambda\pi^-$). These angular distributions are given by

$$W(\cos\theta) = 1/2(1 + A\cos\theta) \ ,$$

where θ is the angle between the direction of the intermediate decay baryon (Λ or Ξ) in the Ω^- rest frame and the direction of the final baryon in the (Λ or Ξ) rest frame. The decay asymmetries A are

$$A_\Omega^\Lambda = \alpha_\Omega^\Lambda \cdot \alpha_\Lambda, \qquad A_\Omega^{\Xi^0} = \alpha_\Omega^{\Xi^0} \cdot \alpha_{\Xi^0}$$

and

$$A_\Omega^{\Xi^-} = \alpha_\Omega^{\Xi^-} \cdot \alpha_{\Xi^-} \ ,$$

respectively. For α_Λ and α_{Ξ^-}, the following values were used: $\alpha_\Lambda = 0.647 \pm 0.014$, $\alpha_{\Xi^-} = -0.411 \pm 0.022$, $\alpha_{\Xi^0} = -0.436 \pm 0.019$. These values were obtained by averaging refs. [8-17].

The decay angular distributions $W(\cos\theta)$ are shown in figs. 22a,b,c for the three decay modes. The full histograms represent the data samples and the dots were obtained from the MC simulation with $\alpha_\Omega = 0$. For the $\Omega^- \to \Lambda K^-$ decay mode (fig. 22a) the data include (307 ± 37) $\Omega^- \to \Xi^0\pi^-$ and (60 ± 8) $\Xi^- \to \Lambda\pi^-$ background events. In the MC distribution the appropriate numbers of MC events satisfying the (ΛK^-) selection criteria were statistically added for those two decays, to take into account the residual background. The effect on the asymmetry was negligible. For the $\Omega^- \to \Xi\pi$ decay modes (figs. 22b and c) the background was subtracted from the data as described in subsection 3.3.2. The dashed histograms correspond to the background distributions.

The values of A obtained from the fits between data and Monte Carlo are

$$\begin{aligned} A_\Omega^\Lambda &= -0.016 \pm 0.018 \\ A_\Omega^{\Xi^0} &= -0.036 \pm 0.051 \\ A_\Omega^\Xi &= -0.020 \pm 0.090 \ . \end{aligned}$$

The errors are statistical only.

Systematic uncertainties arose from several sources. Uncertainties in the measurement of the efficiencies of the drift chambers (DC0-DC4) in the beam region give rise to

$$\delta A_\Omega^\Lambda = 0.004 \qquad \text{and} \qquad \delta A_\Omega^\Xi = 0.002 \ .$$

The background subtraction is a source of possible systematic error only for the $\Omega^- \to \Xi^0\pi^-$ decay mode, where the slope of the background (see fig. 22b) is rather different from that of the signal. The uncertainty in the background subtraction gives $\delta A_\Omega^{\Xi^0} = 0.008$. The uncertainty $\delta p/p = 0.5\%$ on the average beam momentum contributes $\delta A_\Omega^\Lambda = 0.002$, $\delta A_\Omega^{\Xi^0} = 0.022$, and $\delta A_\Omega^\Xi = 0.005$.

The total systematic errors in the asymmetries A were thus estimated to be $\delta A_\Omega^\Lambda = 0.005$, $\delta A_\Omega^{\Xi^0} = 0.023$, and $\delta A_\Omega^\Xi = 0.006$.

Using the values given earlier for α_Λ and α_Ξ, we obtain

$$\begin{aligned} \alpha_\Omega^\Lambda &= -0.025 \pm 0.028 \\ \alpha_\Omega^{\Xi^0} &= 0.09 \pm 0.14 \\ \alpha_\Omega^\Xi &= 0.05 \pm 0.21 \ . \end{aligned}$$

The quoted errors include the estimated systematic uncertainties.

A result, $\alpha_{\Omega}^{\Lambda} = 0.06 \pm 0.14$, from the earlier hyperon-beam experiment was given at the Tokyo Conference [18]. This measurement is superseded by the present result where the systematic uncertainties are much better understood.

4. Ω RARE DECAY MODES

4.1 Search for $\Omega^- \to \Xi^0 e^- \bar{\nu}$

The decay cascade corresponding to this mode is

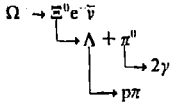

The incoming beam particle and all the decay products, with the exception of the antineutrino, could be measured in the apparatus. The directions and the momenta of the charged decay particles were obtained from the magnetic spectrometer information and the energy of the electron was measured in the lead-glass array. For the γ-rays converted in the lead/MWPC sandwich placed in front of the lead-glass array, the coordinates of the conversion points were measured in the MWPC and the energies in the lead glass. It was thus possible to reconstruct the Ξ^0 by choosing its decay-point position z_{Ξ^0} ($z_{\Omega^-} < z_{\Xi^0} < z_{\Lambda^0}$) such that the effective $\Lambda\gamma\gamma$ mass be the closest approximation to m_{Ξ^0}. This procedure was applied to the $\Xi^0\pi^-$ data sample and fig. 23 shows the $\Lambda\gamma\gamma$ mass distribution thus obtained. The observed width is 4 MeV/c^2 (FWHM) and for 84% of the reconstructed events the $\Lambda\gamma\gamma$ mass is within $\pm$20 MeV/c^2 of the Ξ^0 mass. However, owing to the limited geometrical acceptance for the γ rays, the $\Lambda\gamma\gamma$ reconstruction efficiency alone was only 44%. Therefore the $\Lambda\gamma\gamma$ mass reconstruction was not required for the initial stages of the $\Omega^- \to \Xi^0 e^- \bar{\nu}$ search.

The candidates were first required to satisfy the basic selection criteria described in section 3.1.1. In addition to the beam track and the Λ thus obtained, a negative track, the electron candidate, was required. The intersection of that track with the beam track had to be downstream of $z = 1.3$ m, a cut less restrictive than for the other decay modes, to allow for a more detailed study of the background and a better determination of the signal.

An important source of background was due to cases where a π^0 produced within the event gave an electron through Dalitz decay or γ-ray conversion. These events originated from the $\Omega^- \to \Xi\pi$ decay modes or from beam particle interactions upstream of the (DC0-DC4) drift chambers, in which additional tracks were produced. It was therefore required that there be exactly three charged tracks reconstructed in (DC0-DC4). Because of random or duplicate tracks in the drift chambers, this requirement rejected also a large fraction of the genuine $\Omega^- \to \Xi^0 e^- \bar{\nu}$ decays. The efficiency of the cut was taken to be equal to the value found for the $\Omega^- \to \Xi^0\pi^-$ channel: 48%.

The hadronic background was reduced by using the information from the electron detectors: the lead-glass array and the transition radiation detector (XTRM) shown in fig. 2. The performance of these electron detectors is described in detail elsewhere [4]. The minimal electron selection requirement for the additional negative track was that the ratio between the energy deposited in the

first layer of the lead-glass array and the track momentum be larger than 0.52. After applying this cut there were 511 events in the sample (sample 1). This minimal electron selection was applied to all the subsequent samples and, in addition, more stringent electron cuts were based upon two other requirements for that negative track.

XTR condition: a signal was required in the XTRM. This was 81% efficient for electrons while rejecting hadrons by a factor of about 20.

Lead-glass condition: the ratio between the sum of the energies deposited in the first two layers of the lead-glass array and the track momentum was required to be larger than 0.81.

The hadron rejection obtained with the full lead-glass requirement was 1000:1, uncorrelated with the XTRM rejection, with an electron efficiency of 89%. With all requirements applied the rejection was thus 20,000:1 for an electron efficiency of 72%.

Three more samples were defined by applying to the events of sample 1 additional electron conditions: sample 2 with the XTR condition; sample 3 with the lead-glass condition; sample 4 with both the XTR and the lead-glass conditions. Table 5 gives the number of events in each sample and their evolution when additional criteria described below were applied.

The MC simulation program was used to produce $\Omega^- \to \Xi^0 e^- \bar{\nu}$ events which were analysed with the same set of programs as for the data. Figure 24 shows the distribution of z_Λ, the position of the Λ decay vertex, for the four data samples and for the MC events. The distribution for sample 1, which is mainly background, is peaked at small z_Λ values, whereas, owing to the sequential decay chain $\Omega^- \to \Xi^0 \to \Lambda$, the $\Omega^- \to \Xi^0 e^- \bar{\nu}$ events are concentrated towards larger z_Λ values. As the main background was caused by interactions in the DISC region, it was also concentrated towards small z_{Ω^-} values. Therefore the two-dimensional distribution $(z_\Lambda - z_{\Omega^-}, z_{\Omega^-})$ of the samples was used to evaluate the semi-leptonic signal and the background in the data samples. Let $N_1(i)$ be the number of events in the i^{th} bin for sample 1, and $N_2(i)$ be the corresponding number of events for sample 2; then the signal S_2 and the background $B_2 = \sum_i B_2(i)$ were determined by a least squares fit using the set of equations:

$$N_1(i) = d(i) \cdot S_2/\varepsilon + yB_2(i)$$
$$N_2(i) = d(i) \cdot S_2 + B_2(i) \ ,$$

where $\varepsilon = 0.81$ was the efficiency of the XTRM and y the rejection of the XTRM for the corresponding sample. S_2, B_2, and y were varied. The distribution d(i) of the signal was obtained from the MC events. The same type of equations were used for samples 3 and 4. The results of the two fits were:

$$S_2 = 12.8 \pm 7.2 \ , \quad B_2 = 27.2 \mp 7.2 \ , \quad y = 18.2 \ ,$$
$$S_4 = 14.1 \pm 6.5 \ , \quad B_4 = 16.9 \mp 6.5 \ , \quad y = 11.6 \ .$$

For electrons, the lead-glass condition had an efficiency close to 100%. Therefore one expected $S_4 \simeq S_2$, in agreement with the fit results, whereas the background varied by almost a factor of 2 between the two samples.

The background contributions from the Ω^- main decay modes were evaluated from the data. None of the events of the main decay modes satisfied the electron-selection criteria. Therefore, as it

was required that there be exactly 3 tracks in (DC0-DC4), the main decay modes could only contribute if that negative track had not been reconstructed and there was one extra negative track in the event which had in addition to satisfy the electron criteria. In the data samples there were, amongst the events with 4 reconstructed tracks, no $\Omega^- \to \Lambda K^-$, 4 $\Omega^- \to \Xi^0\pi^-$, and no $\Omega^- \to \Xi^-\pi^0$ which satisfied the electron cuts for the extra negative track. Taking into account the chamber and geometrical efficiencies, we estimated that there were no $\Omega^- \to \Lambda K^-$, 0.4 $\Omega^- \to \Xi^0\pi^-$, and 0.15 $\Omega^- \to \Xi^-\pi^0$ background events. The last number was obtained from the measured ratio $R_2 = (\Gamma(\Omega^- \to \Xi^0\pi^-)/\Gamma(\Omega^- \to \Xi^-\pi^0) = 2.65$. These contributions were already taken into account by the fitting procedure with the exception of that from $\Omega^- \to \Xi^0\pi^-$ decays for which the z_Λ and z_Ω distributions are similar to those from $\Omega^- \to \Xi^0 e^-\bar{\nu}$ decays.

The signal determination was checked by applying additional cuts. Columns 2-4 of Table 5 give the observed numbers of events in samples 1-4 for:

- $z_\Omega > 2$ m ,
- $z_\Omega > 2$ m and $r_\gamma = E_{LG}/(E_{\pi^0} + E_\nu) > 0.3$,
- $z_\Omega > 2$ m and a reconstructed Ξ^0 mass within ± 20 MeV/c^2 of m_{Ξ^0},

where the quantity E_{LG} is a measure of the energy deposited in that region of the lead-glass array that can be reached by γ-rays from the $\Omega^- \to \Xi^0$ decay chain, and $E_{\pi^0} + E_\nu$ is defined as $E_\Omega - E_e - E_\Lambda$.

We then estimated the expected numbers of signal and background events in samples 2 and 4 surviving the additional cuts by the following method. A common value S = 14.1 was assumed for samples 2 and 4 without additional cuts, corresponding to $B_2 = 25.9$ and $B_4 = 16.9$. The efficiencies of the additional cuts for the signal were derived from the $\Omega^- \to \Xi^0\pi^-$ data sample, using an appropriate scaling for r_γ to take into account the neutrino energy in the $\Omega^- \to \Xi^0 e^-\bar{\nu}$ decay. The resulting estimates for the signal after cuts are given in columns 2-4. The background suppressions due to the cuts were assumed to be the same for sample 2(4) as for sample 1(3). They were given in each case by the ratio between the numbers $(N_{1(3)} - S/\varepsilon)$ without and with the additional cuts, where N is the observed number of events and S the expected signal. From these suppressions and from the number of background events before cuts, $B_2 = 25.9$ and $B_4 = 16.9$, we obtained the expected background values listed in columns 2-4.

The observed numbers of events and the expected sums S+B agree in both samples 2 and 4 and for all cuts, although the ratio S/B varies by a factor of 6. For instance, for column 3 of table 5 in the case of sample 4, if there were no $\Omega^- \to \Xi^0 e^-\bar{\nu}$ signal instead of the assumed S = 14.1, one would expect 9.2 ± 2.8 events whereas 17 events are observed. The agreement is taken as a confirmation of the initial signal determination.

Figure 25a shows the (Λe^-) effective mass distribution for sample 4 with $z_\Omega > 1.3$ m (31 events, column 1 of Table 5). Figure 25b shows the same sample with $z_\Omega > 2$ m and $r_\gamma > 0.3$ (17 events, column 3 of Table 5). The curves represent the MC distributions normalized to the calculated $\Omega^- \to \Xi^0 e^-\bar{\nu}$ signals.

The various checks confirm the initial signal determination. The semi-leptonic branching ratio was calculated from $S_4 = 14.1 \pm 6.5$ events minus 0.4 $\Omega^- \to \Xi^0\pi^-$ background events:

$$R = \Gamma(\Omega^- \to \Xi^0 e^-\bar{\nu})/\Gamma\Omega^- \to \text{all}) = (S_4 - 0.4)\cdot BR(\Lambda K^-)/(a\cdot\varepsilon_3\cdot\varepsilon_e\cdot N_{\Lambda K^-}) ,$$

where a = 0.41 was the acceptance relative to the decay $\Omega^- \to \Lambda K^-$, $\varepsilon_3 = 0.48$ the relative efficiency of the 3 tracks requirement, $\varepsilon_e = 0.72$ the electron selection efficiency, and $N_{\Lambda K^-} = 11{,}715$ events, BR (ΛK^-) = 0.675. The uncertainties on these numbers are negligible compared to the error on S_4.

We thus obtained

$$R = (0.56 \pm 0.28) \times 10^{-2} ,$$

where the quoted error includes the uncertainty of the signal determination and that due to the statistical size of the sample.

4.2 Search for $\Omega^- \to \Xi^- \pi^+ \pi^-$

The decay $\Omega^- \to \Xi^- \pi^+ \pi^-$ is different from all the other decay modes studied here in that it produces five charged tracks in the spectrometer. We searched for this decay by selecting all events with a reconstructed Ξ^- and with at least two other charged tracks. The general selection criteria (subsection 3.1) were applied with the exception of the wire multiplicity cut in the third beam chamber.

For the Ω^- vertex, we required that the intersections of the beam with the reconstructed Ξ^- track and the tracks of the two additional particles of opposite charge be compatible within errors. For all those intersections we then required, within reconstruction errors, $z_{\Omega^-} < z_{\Xi^-} < z_\Lambda$, where z_Λ and z_{Ξ^-} refer to the Λ and Ξ^- decay vertices, respectively, and furthermore $z_{\Omega^-} + 2\,\delta z_{\Omega^-} > 2$ m. The effective masses had to fulfil the conditions

$$| m_{p\pi^-} - m_\Lambda | < 10\ \mathrm{MeV/c^2}, \qquad | m_{\Lambda\pi^-} - m_{\Xi^-} | < 18\ \mathrm{MeV/c^2} .$$

The difference Δp_L between the beam momentum and the sum of the longitudinal momenta of the decay particles had to be $|\Delta p_L| < 18$ GeV/c. The width of the Δp_L distribution was estimated to be 3.8 GeV/c (r.m.s.). Out of 25,400 events with at least five reconstructed tracks and the effective mass $m_{\Xi^-\pi^+\pi^-}$ within ± 50 MeV/c^2 of the Ω^- mass, only 5 events remained, all with more than one track combination satisfying all criteria.

A possible contribution to these events could be $\Omega^- \to \Xi^- \pi^0$ decays with a subsequent Dalitz decay or γ-ray conversion. Since the opening angle of the produced e^+e^- pair would be close to zero, this background is strongly suppressed by the requirement, which is part of the event selection, that the π^+ and π^- be different tracks in both sets of drift chambers ($DC_{0,4}$ and $DC_{5,8}$). We used the information from the lead-glass array and the lead/MWPC sandwich as well as the XTRM detector to reject the residual background events, excluding all track combinations for which the π^+ or the π^- candidate had an electron signature. For two events the pion candidates were identified as e^+e^- pairs. Three events remained, where all tracks of the event pointed to the electron detector, but had no electron signature. From the known electron-detection efficiency, the background from Dalitz decays and γ conversions in this sample was estimated to be less than 0.05 events.

Finally we selected the best track combination per event on the basis of the effective masses $m_{p\pi^-}$ and $m_{\Lambda\pi^-}$, the momentum balance Δp_L and the geometrical properties of the Ω^- vertex. The effective masses ($\Xi^-\pi^+\pi^-$) and ($\Xi^-\pi^+$) for these best combinations were 1680, 1686, and 1697 MeV/c^2 (i.e. within ± 15 MeV/c^2 of the Ω^- mass), and 1487, 1525, and 1508 MeV/c^2, respectively. The measurement accuracies on $m_{\Xi^-\pi^+\pi^-}$ and $m_{\Xi^-\pi^+}$ were estimated to be 7 MeV/c^2 and 6 MeV/c^2 (FWHM), respectively, from a MC calculation.

The branching ratio obtained from the three observed events is

$$R = \Gamma(\Omega^- \to \Xi^-\pi^+\pi^-)/\Gamma(\Omega^- \to \text{all}) = (3.7^{+3.6}_{-1.1}) \times 10^{-4} \ .$$

One event with $m_{\Xi^-\pi^-} = 1533$ MeV/c^2 corresponding to a branching ratio 9×10^{-4} was found in the sample collected at 98 and 115 GeV/c. The combined result is then:

$$R = (4.3^{+3.4}_{-1.3}) \times 10^{-4} \ .$$

Theoretical expectations [19] are that the $\Omega^- \to \Xi^-\pi^+\pi^-$ decays should occur mainly via the $\Omega^- \to \Xi^{*0}(1530)\pi^-$ decay mode. It is important to note that for this decay, because of the limited phase space, the average Ξ^{*0} observed mass would be decreased by roughly 12 MeV/c^2, with about 10% of the events having a mass smaller than 1500 MeV/c^2. Therefore the 4 events are consistent with the $\Omega^- \to \Xi^{*0}(1530)\pi^-$ hypothesis. We shall discuss further the $\Omega^- \to \Xi^{*0}\pi^-$ decay rate in section 5, where a comprehensive discussion of the Ω^- decay results will be presented.

4.3 Search for $\Omega^- \to \Xi^-\gamma$

The selection criteria used in this case were the same as for the $\Omega^- \to \Xi^-\pi^0$ decay mode (see subsection 3.1.4) except for the missing-mass cut. The momentum $\vec{p}$ of the γ-ray was defined as the difference between the Ω^- and the Ξ^- momenta. Only events with this vector momentum pointing towards the lead-glass array were retained and it was required that the ratio E_1/p between the energy deposited in the first layer of the array and the γ-ray momentum be larger than 0.39. This cut had an efficiency of 98% for single γ-rays. Additional information on the γ-ray conversion point was provided by the lead/MWPC sandwich situated just in front of the lead-glass array. The distance D between the predicted impact point of the γ-ray and the closest reconstructed hit in the lead/MWPC sandwich was calculated. For $\Omega^- \to \Xi^-\gamma$ decays, owing to the measurement errors on the transverse components of $\vec{p}$, the average value of D was expected to be (80/p) cm with p in GeV/c. It was required that the product (D · p) be smaller than 160 cm · GeV/c corresponding to a 25% loss. Figure 26 shows the distribution of the $(\Omega^- - \Xi^-)$ missing mass squared for the 71 selected events. The two curves on the figure were obtained from the MC simulation of $\Omega^- \to \Xi^-\pi^0$ and $\Omega^- \to \Xi^-\gamma$ decays. Both curves are normalized to the total number of events. The distributions are consistent with all the events being due to $\Omega^- \to \Xi^-\pi^0$ decays. A fit of the relative abundance of the two decay modes gave an upper limit of 9 $\Omega^- \to \Xi^-\gamma$ events at the 90% confidence level.

The $\Omega^- \to \Xi^-\gamma$ acceptance relative to $\Omega^- \to \Lambda K^-$ was found to be 0.31 from a MC calculation. Taking into account the 90% conversion probability and the 87% detection efficiency of the γ chambers, the total γ-ray detection efficiency was $\varepsilon_\gamma = 76\%$. Thus, from the upper limit of 9 $\Omega^- \to \Xi^-\gamma$ events, we obtained, by using the number of events and the branching ratio of the (ΛK^-) channel (Table 4):

$$\Gamma(\Omega^- \to \Xi^-\gamma)/\Gamma(\Omega^- \to \text{all}) < 2.2 \times 10^{-3} \text{ at the 90\% confidence level} \ .$$

This is to be compared with the limit of 3.1×10^{-3} obtained in the previous hyperon beam experiment [2].

4.4 Search for $\Omega^- \to \Lambda\pi^-$

We have made a search for the $\Delta S = 2$ decay $\Omega^- \to \Lambda\pi^-$ by applying all cuts used for the $\Omega^- \to \Lambda K^-$ sample (see subsection 3.1.2) with the exception of the requirement on the effective mass $m_{\Lambda K^-}$. Instead we required the effective mass $m_{\Lambda\pi^-}$ obtained by interpreting the additional negative particle as a π^- to be within ± 60 MeV/c^2 of the Ω^- mass. There remained 9 events (see fig. 27), two of them within 18 MeV/c^2 of the Ω^- mass. One of these two events has $m_{\Lambda K^-} = 1674$ MeV/c^2 for a different track combination and is therefore rejected. The remaining event has a missing longitudinal momentum $\Delta p_L \simeq p_L^{\Omega^-} - p_L^{\Lambda} - p_L^{\pi^-} = 9.94$ GeV/c. Discarding this event, which has a longitudinal momentum imbalance of 2.8 standard deviations, we calculate an upper limit on the branching ratio

$$\Gamma(\Omega^- \to \Lambda\pi^-)/\Gamma(\Omega^- \to \text{all}) < 1.9 \times 10^{-4} \text{ at the 90\% confidence level} .$$

This is seven times lower than the previous limit of 1.3×10^{-3} (ref. [2]).

5. DISCUSSION AND CONCLUSIONS

In this section we discuss the impact of our results on various theoretical predictions. For the purpose of these comparisons we have combined the results of the present experiment with those measured in the previous experiment at the SPS hyperon beam.

- The Ω^- lifetime is $\tau_{\Omega^-} = (0.823 \pm 0.013) \times 10^{-10}$ s.
- The parameters of the Ω^- main decay modes are given in Table 6.
- The ratio of the $\Omega^- \to \Xi\pi$ decay rates is

$$R_2 \simeq \Gamma(\Omega^- \to \Xi^0\pi^-)/\Gamma(\Omega^- \to \Xi^-\pi^0) = 2.72 \pm 0.17 .$$

Taking into account the phase-space difference between the two $\Omega^- \to \Xi\pi$ modes, a pure $|\Delta I| = 1/2$ transition amplitude would give $R_2 = 2.07$, which differs by 3.8 standard deviations from the experimental result. From the value of R_2 we obtain the ratio between the $|\Delta I| = 3/2$ and the $|\Delta I| = 1/2$ amplitude:

$$A_3/A_1 = -0.063 \pm 0.014.$$

The dominance of the $|\Delta I| = 1/2$ amplitude in the non-leptonic decays of kaons and octet hyperons has been studied extensively and, using the QCD framework, a coherent description of these decays has emerged [20,21]. The same formalism has been applied to Ω^- decays by several authors [19, 22-24]. The elementary quark operator in the strangeness changing transition corresponds to the scattering process $s + u \to u + d$ in which only one strange quark is involved. As the Ω^- contains three strange valence quarks, several diagrams which are present for other hyperon decays do not contribute in the Ω^- case. Since the suppressed diagrams correspond to $|\Delta I| = 1/2$ transitions, the relative contribution of $|\Delta I| = 3/2$ is enhanced.

In the formalism of Shifman, Vainshtein and Zakharov [20] (SVZ), the effective weak Hamiltonian, which includes QCD corrections and SU(4) flavour-symmetry breaking, is of the form:

$$H_W^{eff}(\Delta S = 1) = \sqrt{2}\, G_F \sin\theta_C \cos\theta_C \sum_{i=1}^{i=6} C_i O_i \ .$$

The O_i are four-quark operators. They all correspond to $|\Delta I| = 1/2$ weak transitions except for O_4 which is a $|\Delta I| = 3/2$ operator. C_5 and C_6 are zero in the absence of SU(4) flavour-symmetry breaking.

A prediction of the model, independent of the values of the coefficients C_i, is that the three main decay modes are dominated by P-wave amplitudes [22]. This implies $\alpha_\Omega \simeq 0$, in agreement with the asymmetry parameter measurements (see Table 6). The decay rates are therefore expressed as a function of the P-wave amplitude. The $\Omega^- \to \Xi\pi$ decay rates are thus written as [23]:

$$\Gamma = (G_f^2/4\pi) \sin^2\theta_C \cos^2\theta_C\, p_\pi^3 [(E_\Xi + m_\Xi)/24\, m_\Omega\ ] |B|^2 \ .$$

We will use the most recent evaluation of B by Lusignoli and Pugliese [24]. It can be written as

$$B = K(B_{pole} + H[-C_1 + 2(C_2 + C_3) - P + d\cdot C_4]) \ ,$$

where B_{pole} is the contribution of the pole terms and P that from the "penguin" diagrams. Both these terms receive contributions only from the operators O_5 and O_6, in particular P is proportional to $(C_5 + 3/16\, C_6)$. For $\Omega^- \to \Xi^0\pi^-$, K = 1, d = 2 and for $\Omega^- \to \Xi^-\pi^0$, $K = 1/\sqrt{2}$, d = −4. The expressions for B_{pole}, P, and H are given in ref. [24]. The pole contribution is about 15% of the other term. The values of the coefficients C_1, C_2, C_3 and C_4 are only weakly sensitive, via logarithmic corrections, to the value of the mass at which the strong coupling constant $g^2(m)/4\pi$ is equal to 1. For instance, when one varies m from m_ρ to m_π, the quantities $[-C_1 + 2(C_2 + C_3)]$ and C_4 are increased by only about 8% and 5% respectively. On the other hand, C_5 and C_6 which are entirely generated by QCD corrections depend strongly upon the value of m. When m is decreased from m_ρ to m_π the quantity $(C_5 + 3/16 C_6)$ is multiplied by a factor of 2.

We use as input the values $C_1 = -2.8$, $C_2 = 0.06$, and $C_3 = 0.08$, corresponding to $g^2(m)/4\pi = 1$ at the pion mass and we determine C_4 and $(C_5 + 3/16\, C_6)$ using our measurements of the two $\Omega^- \to \Xi\pi$ decay rates. Figure 28 shows the constraints imposed by the rate values in the plane [C_4, $(C_5 + 3/16\, C_6)$]. We obtain the results*):

$$C_5 + 3/16\, C_6 = -0.172 \pm 0.005$$
$$C_4 = 0.261 \pm 0.064 \ .$$

The quoted errors are only those due to the uncertainties on the decay rates.

The value of $(C_5 + 3/16\ C_6)$ is slightly smaller than the theoretical value of −0.15 obtained by SVZ [20] with $g^2(m)/4\pi = 1$ at the pion mass, which may indicate a value of m slightly smaller than m_π. The value of C_4 is significantly smaller than 0.41 which was originally predicted by the model, but it is in excellent agreement with the value $C_4 = 0.25$ needed to fit the pure $|\Delta I| = 3/2$ $K^+ \to \pi^+\pi^0$ decay amplitude [21].

*) We used the values 0.122 GeV for H and 10.9 for the penguin enhancement factor, $m_\pi^2/[(m_u + m_d)(m_s + m_u)]$.

The $\Omega^- \to \Lambda K^-$ decay amplitude calculated with the values of the coefficients C_i given above is 25% smaller than the experimental result. This amplitude is dominated by a $(\Omega^-\Xi^0K^-)$ pole term whose contribution is subject to a theoretical uncertainty which might well be as large as the above discrepancy.

From this comparison of the experimental parameters for the Ω^- main decay modes with the theoretical predictions, we conclude that the SVZ model is rather successful at describing the enhancement of the $|\Delta I| = 1/2$ amplitude by the penguin diagrams, whose contributions correspond to about 75% of the $\Omega^- \to \Xi\pi$ decay amplitudes. The suppression of the $|\Delta I| = 3/2$ amplitude by about a factor of 1.5 with respect to the prediction, which is also found in the case of the $K^+ \to \pi^+\pi^0$ decay, remains to be explained.

The $\Omega^- \to \Xi^*(1530)\pi$ decays are expected to dominate the $\Xi^-\pi^+\pi^-$ decay modes. Assuming that the 4 events are $\Omega^- \to \Xi^{*0}\pi^-$ events, we deduce using a branching ratio of 2/3 for $\Xi^{*0} \to \Xi^-\pi^+$:

$$\Gamma(\Omega^- \to \Xi^{*0}\pi^-)/\Gamma(\Omega^- \to \text{all}) = (6.4^{+5.1}_{-2.0}) \times 10^{-4}$$

$$\Gamma(\Omega^- \to \Xi^{*0}\pi^-) = (7.8^{+6.2}_{-2.4}) \times 10^6\ s^{-1} .$$

Neglecting the contributions of the D- and F-waves, the decay rate can be written as [24]:

$$\Gamma(\Omega^- \to \Xi^{*0}\pi^-) = (G_F m_\pi \sin\theta_C \cos\theta_C/2\sqrt{2})^2 \cdot (p_{\Xi^*}/18\pi m_\eta)(k^+|A|^2 + k^-|B|^2) ,$$

where

$$k^\pm = (E_{\Xi^*} \pm m_{\Xi^*})[(E_{\Xi^*}/m_{\Xi^*})^2 \pm (E_{\Xi^*}/m_{\Xi^*}) + 5/2] .$$

The dominant contributions to the amplitudes A (S-wave) and B (P-wave) were first derived by Finjord and Gaillard [19]. To calculate the decay rate we have used the more complete expressions of Lusignoli and Pugliese [24] which include the pole term and commutator contributions. The input parameters for the Ξ^{*0} resonance were a central mass value of $(1531.8 \pm 0.34)\ MeV/c^2$ and a width of $9.14\ MeV/c^2$. The distortion of the Breit-Wigner due to the P-wave decay amplitude of the Ξ^* was also taken into account. Using the values given earlier for the coefficients C_i, we obtained

$$\Gamma(\Omega^- \to \Xi^{*0}\pi^-) = (\quad \pm 11) \times 10^6\ s^{-1} ,$$

where the contributions to the quoted theoretical uncertainty are (in units of $10^6\ s^{-1}$): 8 due to δm_η and δm_{Ξ^*}, 6 due to δC_4, δC_5, and δC_6, and 4 from the uncertainties on the pole-term contributions. The S (P) wave partial decay rates are 33 (8) $\times 10^6\ s^{-1}$.

It should be noted that the relative sign of the penguin and non-penguin amplitudes is the same in P-wave $\Xi\pi$ and $\Xi^{*0}\pi^-$ decays, but changes in S-wave $\Xi^{*0}\pi^-$ decays. Thus a small change in the parameters C_i, which would hardly affect the $\Omega^- \to \Xi\pi$ decay rates or the $\Omega^- \to \Xi^{*0}\pi^-$ P-wave partial decay rate, will strongly affect the $\Omega^- \to \Xi^{*0}\pi^-$ S-wave amplitude A, and this effect is magnified by the kinematic factor k^+ (which is much bigger than k^-).

In conclusion, the theoretical estimate of the $\Omega^- \to \Xi^{*0}\pi^-$ decay rate appears to be significantly larger than the experimental result. However, the quoted theoretical uncertainty, which includes only the effects listed above, is likely to be an underestimate.

The theoretical predictions on weak radiative decays have been recently reviewed by Kogan and Shifman [25]. The $\Omega^- \to \Xi^- \gamma$ branching ratio is expected to be $(1-1.5) \times 10^{-5}$, about two orders of magnitude lower than the experimental upper limit of $\simeq 2 \times 10^{-3}$.

Finally, the value obtained for the $\Omega^- \to \Xi^0 e^- \bar{\nu}$ branching ratio, $R = (0.56 \pm 0.28) \times 10^{-2}$ is in agreement with the theoretical prediction [19] of about 1×10^{-2}.

Acknowledgements

We wish to thank Mary K. Gaillard for her very valuable advice, and Roberto Petronzio and Maurizio Lusignoli for important clarifying discussions. We gratefully acknowledge the support given by the Centre de Calcul de Physique Nucléaire (CCPN) Paris.

REFERENCES

1. M. Bourquin et al., Phys. Lett. **87B** (1979) 297.
2. M. Bourquin et al., Phys. Lett. **88B** (1979) 192.
3. M. Bourquin et al., Nucl. Phys. **B153** (1979) 13.
4. M. Bourquin et al., Nucl. Instrum. Methods **204** (1983) 311.
5. J. Lecoq et al., CRN-HE 78-16 CRN Strasbourg.
6. Particle Data Group, Review of Particle properties, Phys. Lett. **111B** (1982).
7. M. Baubillier et al., Phys. Lett. **78B** (1978) 342.
8. R.J. Hemingway et al., Nucl. Phys. **B142** (1978) 205.
9. P.M. Dauber et al., Phys. Rev. **179** (1969) 1262.
10. C. Baltay et al., Phys. Rev. **D9** (1974) 49.
11. O.E. Overseth and R.F. Roth, Phys. Rev. Lett. **19** (1967) 391.
12. W. Cleland et al., Nucl. Phys. **B40** (1972) 221.
13. G. Bunce et al., Phys. Rev. **D18** (1978) 633.
14. R. Handler et al., Phys. Rev. **D25** (1982) 639.
15. R. Cool et al., Phys. Rev. **D10** (1974) 792.
16. W. Cleland et al., Phys. Rev. D21 (1980) 12.
17. S.F. Biagi et al., Phys. Lett. **112B** (1982) 277.
18. M. Bourquin et al., Contribution No. 776, Proc. 19th Int. Conf. on High Energy Physics, Tokyo, 1978 (Phys. Soc. Japan, Tokyo, 1979), p. 427.
19. J. Finjord and M.K. Gaillard, Phys. Rev. D22 (1980) 778.
20. M.A. Shifman, A.I. Vainshtein and V.I. Zakharov, Nucl. Phys. **B120** (1977) 316 and Preprint ITEP-63 (1976).
21. A.I. Vainshtein, V.I. Zakharov and M.A. Shifman, Preprint ITEP-64 (1976).
22. J. Finjord, Phys. Lett. **76B** (1978) 116.
23. H. Galić, D. Tadić and J. Trampetić, Phys. Lett. **89B** (1980) 249.
24. M. Lusignoli and A. Pugliese, Phys. Lett. 132B (1983) 178.
25. Ya.I. Kogan and M.A. Shifman, Preprint ITEP-34 (1983) and references therein.

Table 1

Results of Ω^- lifetime fits using the decay mode $\Omega^- \rightarrow \Lambda K^-$

z_{min}, z_{max} (m)	Events	τ_Ω (10^{-10} s)	χ^2/DF
2.0, 10.0	13737	0.835 ± 0.011	41.9/38
2.8, 10.0	9875	0.823 ± 0.013	37.8/34
4.4, 10.0	3879	0.813 ± 0.027	28.3/26
2.0, 8.0	13413	0.836 ± 0.013	31.7/28
2.8, 8.0	9551	0.821 ± 0.016	27.6/24

Table 2

Results of Ω^- lifetime fits using the decay mode $\Omega^- \rightarrow \Xi^0\pi^-$

z_{min}, z_{max} (m)	Events	τ_Ω (10^{-10} s)	χ^2/DF
2.0, 8.0	1471	0.833 ± 0.037	30.6/28
2.8, 8.0	1133	0.823 ± 0.047	25.9/24
2.0, 7.0	1433	0.850 ± 0.040	28.7/23
2.8, 7.0	1095	0.840 ± 0.056	24.1/19

Table 3

Results of Ξ^- lifetime fits

z_{min}, z_{max} (m)	Events	τ_Ξ (10^{-10} s)	χ^2/DF
2.0, 12.0	38815	1.613 ± 0.024	47.0/48
2.0, 10.0	37580	1.633 ± 0.027	33.3/38
2.8, 10.0	31817	1.652 ± 0.033	30.1/34
4.4, 10.0	18832	1.617 ± 0.051	19.3/26
2.0, 8.0	34364	1.637 ± 0.036	29.3/28
2.8, 8.0	28601	1.670 ± 0.045	25.8/24

Table 4

Ω^- decay branching ratios

Decay channel	ΛK^-	$\Xi^0\pi^-$	$\Xi^-\pi^0$
Events	11715 ± 116	1630 ± 65	614 ± 37
Relative acceptances	1.0	0.398	0.397
Branching ratios	0.675 ± 0.008	0.236 ± 0.008	0.089 ± 0.005
Results at 98 and 115 GeV/c (ref. 2)	0.686 ± 0.013	0.234 ± 0.013	0.080 ± 0.008

Table 5

Signal and background in $\Omega^- \to \Xi^0 e^- \bar{\nu}$ samples

Samples* \ Cuts	$z_\Omega > 1.3$ m	$z_\Omega > 2$ m	$z_\Omega > 2$ m $r_\gamma > 0.3$	$z_\Omega > 2$ m Ξ^0 mass
1	511	342	126	69
2	40 $S_2 = 12.8 \pm 7.2$ $B_2 = 27.2 \mp 7.2$	30 $S = 13.4$ $B = 17.1$	19 $S = 12.0$ $B = 5.8$	8 $S = 5.4$ $B = 3.3$
3	213	153	63	29
4	31 $S_4 = 14.1 \pm 6.5$ $B_4 = 16.9 \mp 6.5$	26 $S = 13.4$ $B = 11.8$	17 $S = 12.0$ $B = 4.2$	6 $S = 5.4$ $B = 1.9$

* See text for the definition of the electron-selection criteria applied to each of the four samples.

Table 6

The Ω^- main decay modes (combined results)

	Branching ratio	Γ ($10^9 s^{-1}$)	α_Ω
$\Omega^- \to \Lambda K^-$	0.678 ± 0.007	8.24 ± 0.15	-0.025 ± 0.028
$\Omega^- \to \Xi^0 \pi^-$	0.236 ± 0.007	2.87 ± 0.09	0.09 ± 0.14
$\Omega^- \to \Xi^- \pi^0$	0.086 ± 0.004	1.04 ± 0.05	0.05 ± 0.21

Figure captions

Fig. 1 Schematic view of the magnetic channel and beam counters: bending magnets (M1, M2, M3); superconducting quadrupoles (Q1, Q2); horizontally adjustable collimators (C1, C2, C3); beam-defining counters (T0, T1, T2); beam halo veto counters (A1, A2).

Fig. 2 Plan view of the apparatus: helium bag (He); transition radiation detector composed of a lithium radiator (Li) and xenon proportional chambers (Xe); drift chambers (DC)

Fig. 3 Wire multiplicities in the third beam chamber:
a) for beam particles;
b) for reconstructed $\Xi^- \to \Lambda\pi^-$ events;
c) for Ω^- raw data.

Fig. 4 $\Omega^- \to \Lambda K^-$ candidates. $(\Lambda\pi^-)$ effective mass versus (ΛK^-) effective mass for a partial sample (16%).

Fig. 5 $(\Omega^- - \pi^-)$ missing mass versus (ΛK^-) effective mass for the $\Omega^- \to \Lambda K^-$ sample. The horizontal band around the Ξ^0 mass corresponds to $\Omega^- \to \Xi^0\pi^-$ background events.

Fig. 6 (ΛK^-) effective mass for the $\Omega^- \to \Lambda K^-$ sample. The curve represents the corresponding MC distribution. The arrows indicate the mass interval used for the signal determination.

Fig. 7 $\Omega^- \to \Xi^0\pi^-$ candidates. $(\Lambda\pi^-)$ effective mass versus $(\Omega^- - \pi^-)$ missing mass for a partial sample (16%). The curve represents the kinematic boundaries of the $(\Lambda\pi^-\pi^0)$ final state for Ω^- decays.

Fig. 8 $\Omega^- \to \Xi^0\pi^-$ candidates. $(\Lambda\pi^-)$ effective mass versus $(\Omega^- - \pi^-)$ missing mass, for $\Omega^- \to \Xi^0\pi^-$ candidates with additional selection criteria (see subsection 3.1.3). The horizontal band around the Ξ^- mass corresponds to $\Xi^- \to \Lambda\pi^-$ background events.

Fig. 9 (ΛK^-) effective mass versus $(\Omega^- - \pi^-)$ missing mass for the $\Omega^- \to \Xi^0\pi^-$ sample before applying the Ξ^0 mass cut. The horizontal band around the Ω^- mass corresponds to $\Omega^- \to \Lambda K^-$ background events.

Fig. 10 $\Omega^- \to \Xi^0\pi^-$ sample.
a) $(\Omega^- - \Lambda - \pi^-)$ missing mass squared.
b) $(\Omega^- - \pi^-)$ missing mass.
Shaded histograms, events with a γ signal.

Fig. 11 $\Omega^- \to \Xi^-\pi^0$ candidates. $(\Omega^- - \Xi^-)$ missing mass squared versus the missing longitudinal momentum for a partial sample (16%). The full curve shows the kinematic limit. The dashed lines indicate the Δp_L and Δp_T cuts applied for the $\Omega^- \to \Xi^-\pi^0$ selection.

Fig. 12 $\Omega^- \to \Xi^-\pi^0$ sample. $(\Omega^- - \Xi^-)$ missing mass squared versus the missing longitudinal momentum. The dotted lines define the mass interval used for the signal determination.

Fig. 13 $(\Omega^- - \Xi^-)$ missing mass squared for the $\Omega^- \to \Xi^-\pi^0$ sample. The arrows indicate the mass interval used for the signal determination. Shaded histogram, events with a γ signal.

Fig. 14 Percentage of the signal accepted by the lead-glass requirements. The distribution for $\Omega^- \to \Xi^0\pi^-$ has been measured and used as input to deduce the $\Omega^- \to \Xi^-\pi^0$ curve.

Fig. 15 Distribution of the distance R_p between the proton track and the beam axis at $z = 15$ m for $\Xi^- \to \Lambda\pi$, $\Lambda \to p\pi^-$ decays. The histogram represents the data. The dashed curve corresponds to the MC for 100% efficiency in the central region of DC0 to DC4 and the full curve to the MC with adjusted inefficiencies.

Fig. 16 $\Omega \rightarrow \Lambda K$ sample.
a) Distribution of the Λ momentum for data and MC.
b) Distribution of the Λ angle with respect to the beam particle for data and MC.

Fig. 17 $\Omega \rightarrow \Xi^0\pi$ sample.
a) Distribution of the missing longitudinal momentum for signal, background, and MC.
b) Distribution of the π angle with respect to the beam particle for signal, background, and MC.

Fig. 18 $\Omega \rightarrow \Xi\ \pi^0$ sample. Distribution of the missing longitudinal momentum for signal, background, and MC.

Fig. 19 $\Omega \rightarrow \Lambda K$ decay-point distribution. The curve represents the result of the lifetime fit. The arrows indicate the interval used for the fit. The inset shows the variation of χ^2 (for 34 degrees of freedom) with the Ω lifetime.

Fig. 20 a) $\Omega \rightarrow \Xi^0\pi$ decay-point distribution, after subtraction of the background shown by the dotted histogram. The curve represents the result of the lifetime fit. The arrows indicate the interval used for the fit.
b) $\Omega \rightarrow \Xi\ \pi^0$ decay-point distribution, after subtraction of the background shown by the dotted histogram. The curve represents the result of the lifetime fit. The arrows indicate the interval used for the fit.

Fig. 21 $\Xi \rightarrow \Lambda\pi$ decay-point distribution. The curve represents the result of the lifetime fit. The arrows indicate the interval used for the fit. The inset shows the variation of χ^2 (for 34 degrees of freedom) with the Ξ lifetime.

Fig. 22 a) $\Omega \rightarrow \Lambda K$ sample. Distribution of the cosine of the angle between the direction of the Λ in the Ω rest frame and the proton direction in the Λ rest frame. The points are the MC distribution for $\alpha_\Omega^\Lambda = 0$.
b) $\Omega \rightarrow \Xi^0\pi$ sample. Distribution of the cosine of the angle between the direction of the Ξ^0 in the Ω rest frame and the Λ direction in the Ξ^0 rest frame, after subtraction of the background shown by the dashed histogram. The points are the MC distribution for $\alpha_\Omega^{\Xi^0} = 0$.
c) $\Omega \rightarrow \Xi\ \pi^0$ sample. Distribution of the cosine of the angle between the direction of the Ξ in the Ω rest frame and the Λ direction in the Ξ rest frame, after subtraction of the background shown by the dashed histogram. The points are the MC distribution for $\alpha_\Omega^\Xi = 0$.

Fig. 23 Distribution of the $\Lambda\gamma\gamma$ effective mass for the $\Omega \rightarrow \Xi^0\pi$ sample.

Fig. 24 $\Omega \rightarrow \Xi^0 e\ \bar{\nu}$ candidates. Λ decay point for:
a) samples 1 and 3 (shaded);
b) sample 2;
c) sample 4;
d) MC sample normalized to sample 1.

Fig. 25 $\Omega \rightarrow \Xi^0 e\ \bar{\nu}$ candidates. (Λe) effective mass distribution for:
a) sample 4, column 1 of Table 5.
b) sample 4, column 3 of Table 5.
The shaded events are those satisfying Ξ^0 reconstruction. The curves represent the MC distributions normalized to the signals.

Fig. 26 $\Omega^- \to \Xi^-\gamma$ candidates. Distribution of the $(\Omega^- - \Xi^-)$ missing mass squared. The full (dashed) curve shows the MC prediction for $\Omega^- \to \Xi^-\gamma$ ($\Omega^- \to \Xi^-\pi^0$) decays.

Fig. 27 $\Omega^- \to \Lambda\pi^-$ candidates. Distribution of the $(\Lambda\pi^-)$ effective mass.

Fig. 28 Constraints imposed on C_4 and $(C_5 + 3/16\ C_6)$ by the $\Omega^- \to \Xi^0\pi^-$ (solid line) and the $\Omega^- \to \Xi^-\pi^0$ (broken line) decay amplitudes. The strips correspond to ± 1 standard deviation.

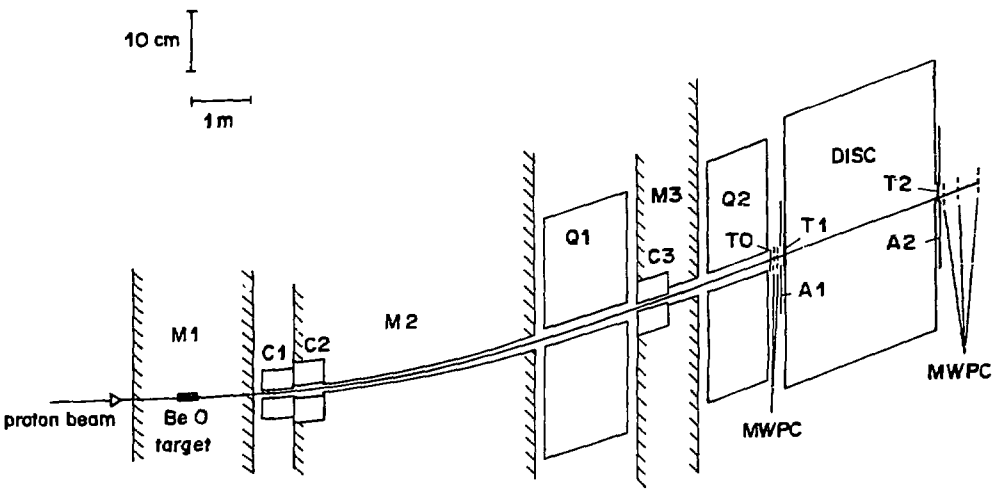
10 cm
1 m
M1
C1
C2
M2
Q1
M3
C3
Q2
TO
T1
A1
DISC
T2
A2
MWPC
MWPC
proton beam
Be O
target

Figure 1

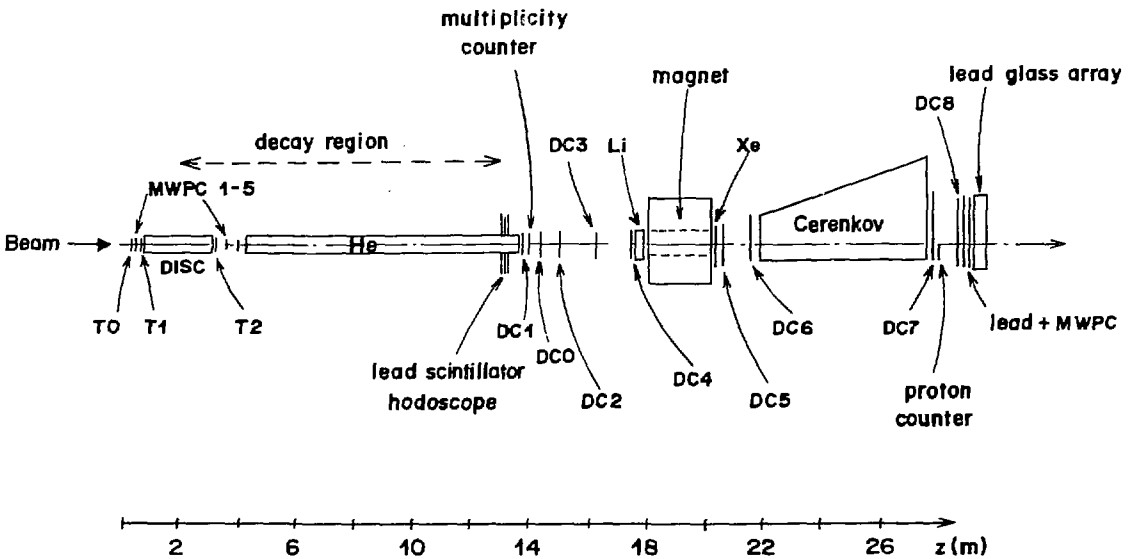
multiplicity
counter
magnet
lead glass array
DC8
decay region
DC3
Li
Xe
MWPC 1-5
Beam
He
Cerenkov
DISC
T0
T1
T2
DC1
DC0
DC2
DC4
DC5
DC6
DC7
lead + MWPC
lead scintillator
hodoscope
proton
counter
2
6
10
14
18
22
26
z (m)

Figure 2

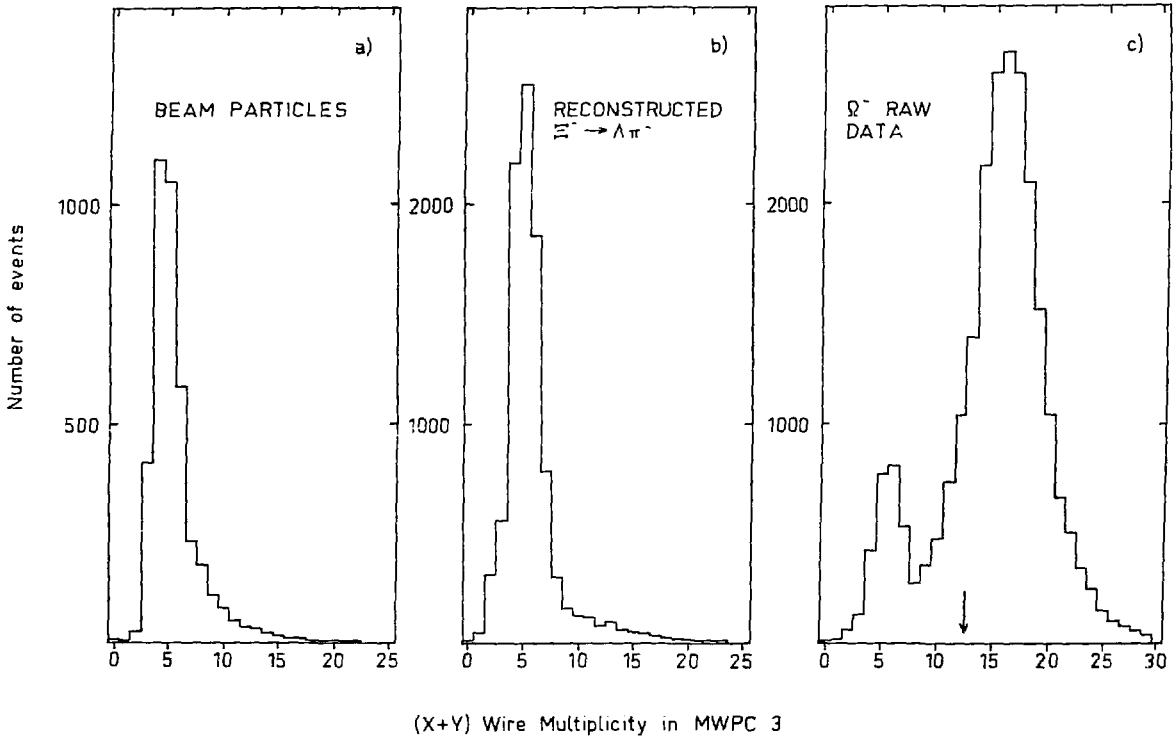
a)
BEAM PARTICLES
b)
RECONSTRUCTED
Ξ⁻ → Λπ⁻
c)
Ω⁻ RAW
DATA
Number of events
1000
500
2000
1000
2000
1000
0 5 10 15 20 25
0 5 10 15 20 25
0 5 10 15 20 25 30
(X+Y) Wire Multiplicity in MWPC 3

Figure 3

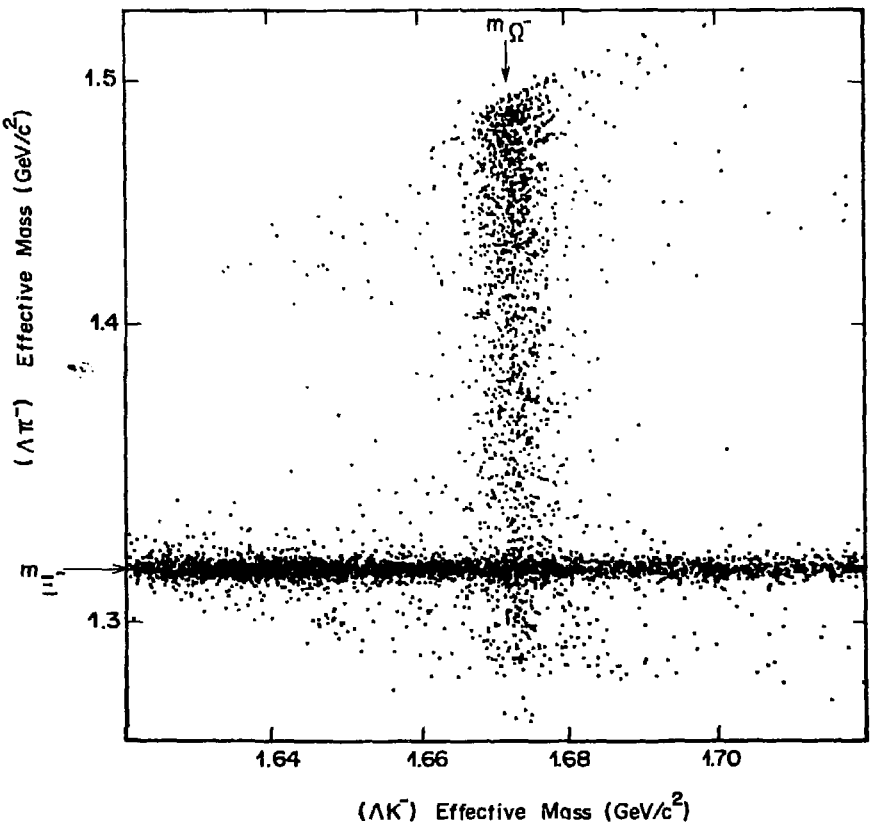
m Ω⁻
1.5
1.4
m Ξ⁻
1.3
(Λπ⁻) Effective Mass (GeV/c²)
1.64
1.66
1.68
1.70
(ΛK⁻) Effective Mass (GeV/c²)

Figure 4

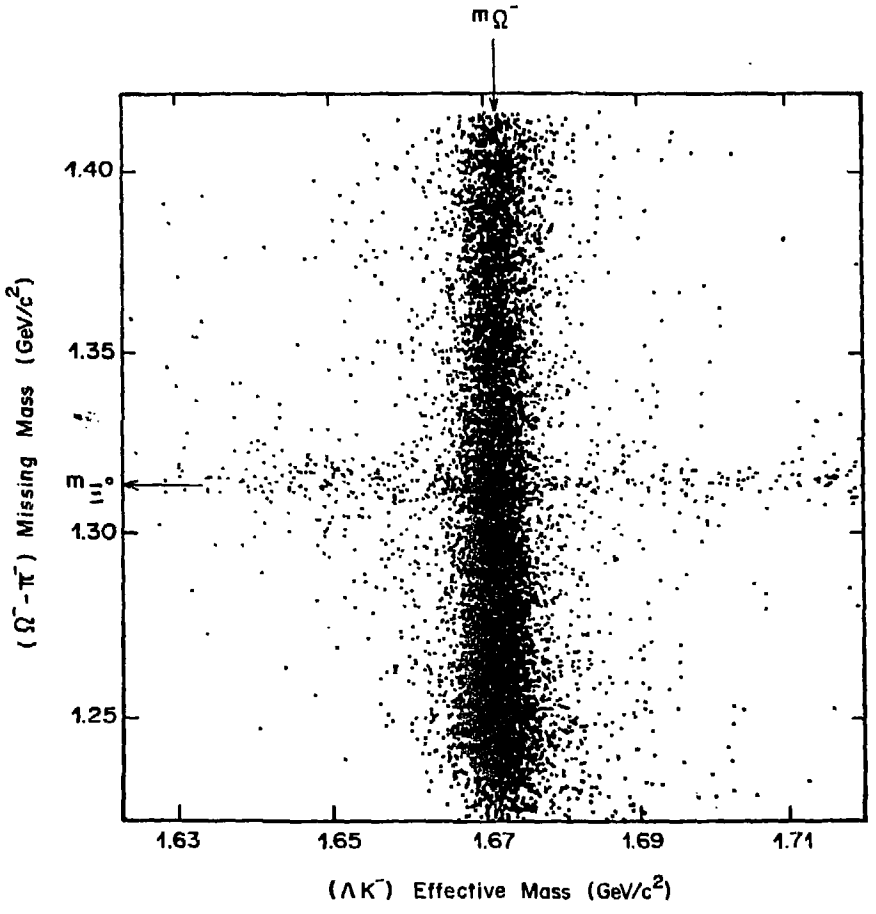
mΩ⁻
1.40
1.35
m Ξ⁰
1.30
1.25
(Ω⁻-π⁻) Missing Mass (GeV/c²)
1.63
1.65
1.67
1.69
1.71
(ΛK⁻) Effective Mass (GeV/c²)

Figure 5

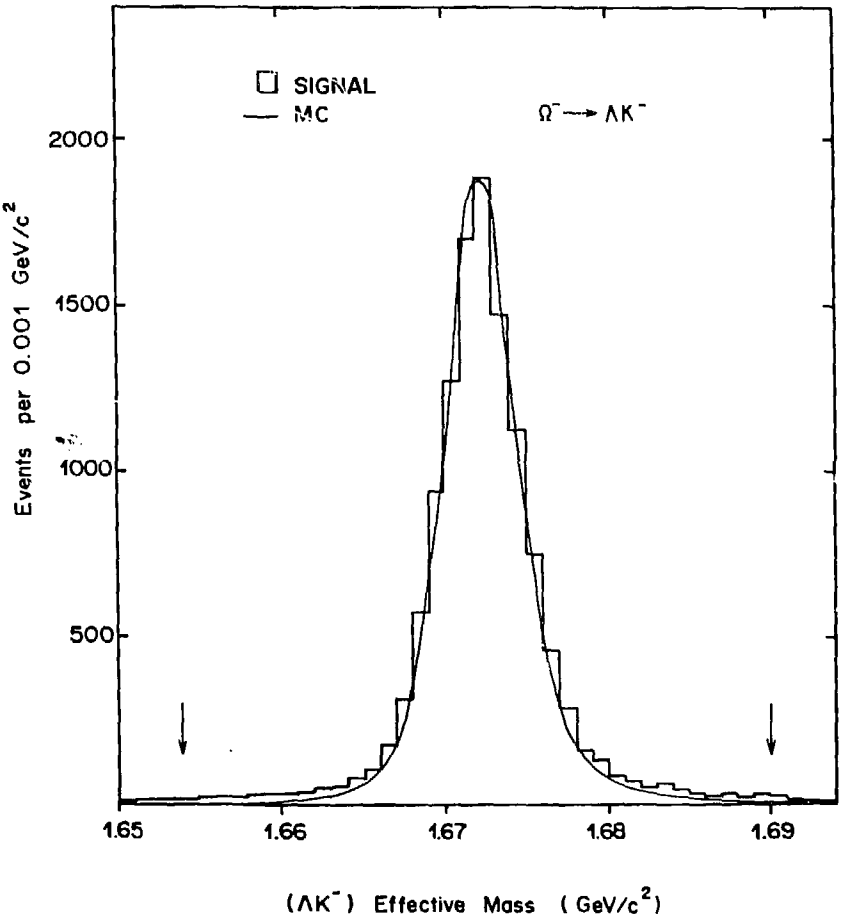
SIGNAL
MC
$\Omega^- \rightarrow \Lambda K^-$
2000
1500
1000
500
Events per 0.001 GeV/c^2
1.65
1.66
1.67
1.68
1.69
(ΛK^-) Effective Mass (GeV/c^2)

Figure 6

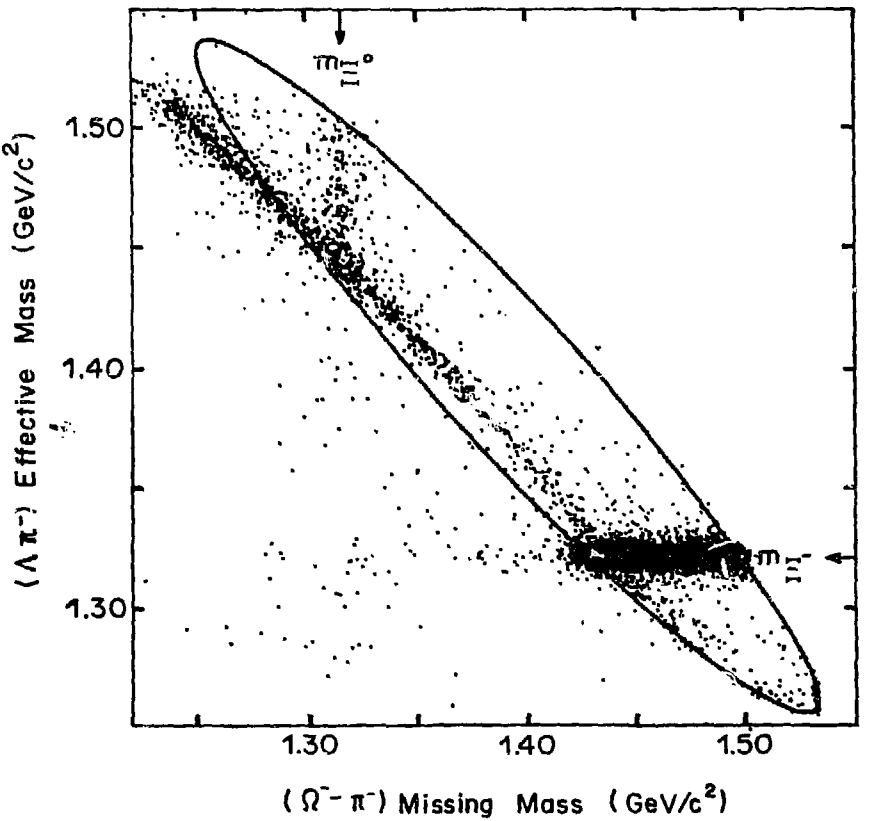
m_{Ξ^0}
m_{Ξ^-}
1.50
1.40
1.30
1.30
1.40
1.50
$(\Lambda\pi^-)$ Effective Mass (GeV/c^2)
$(\Omega^-\pi^-)$ Missing Mass (GeV/c^2)

Figure 7

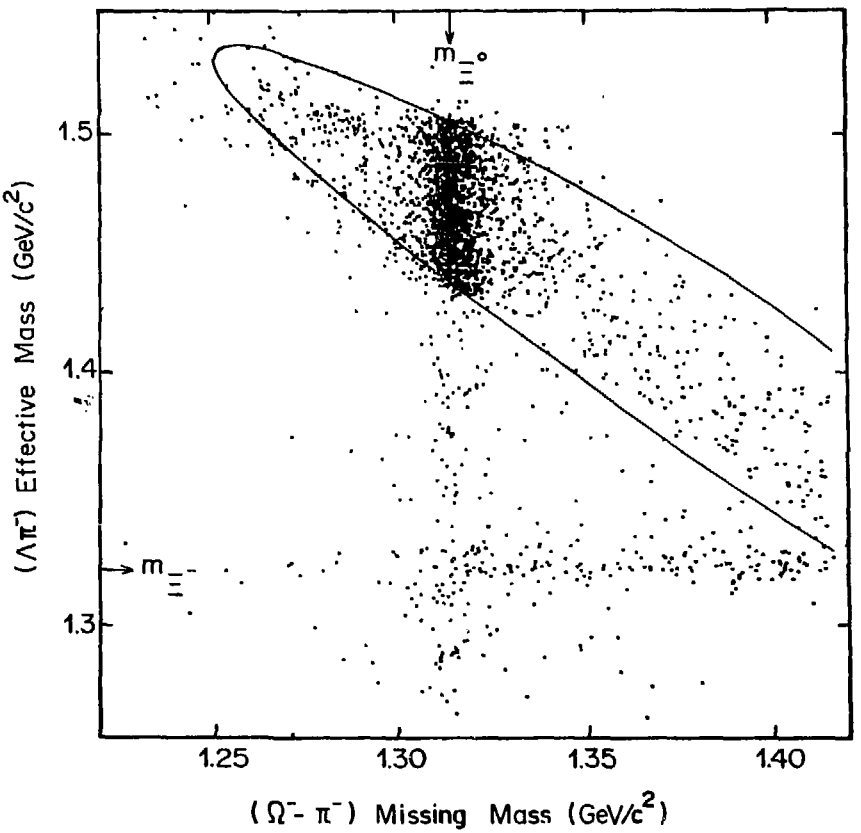
m Ξ°
m Ξ⁻
1.5
1.4
1.3
1.25
1.30
1.35
1.40
(Λπ⁻) Effective Mass (GeV/c²)
(Ω⁻ - π⁻) Missing Mass (GeV/c²)

Figure 8

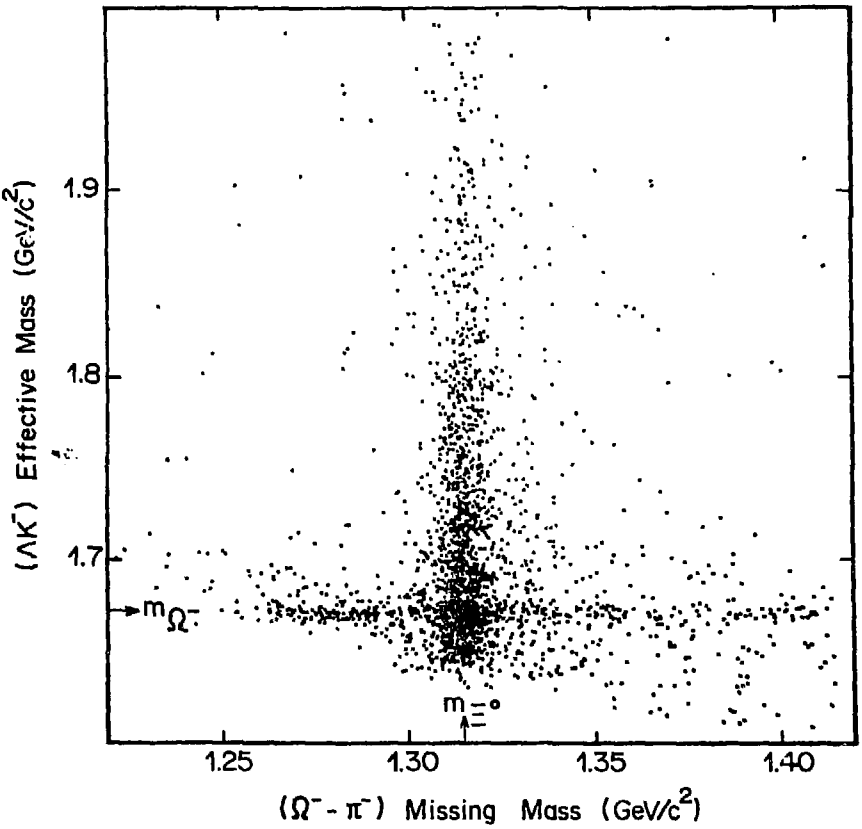
(ΛK⁻) Effective Mass (GeV/c²)
1.9
1.8
1.7
m_Ω⁻
m_Ξ°
1.25
1.30
1.35
1.40
(Ω⁻ - π⁻) Missing Mass (GeV/c²)

Figure 9

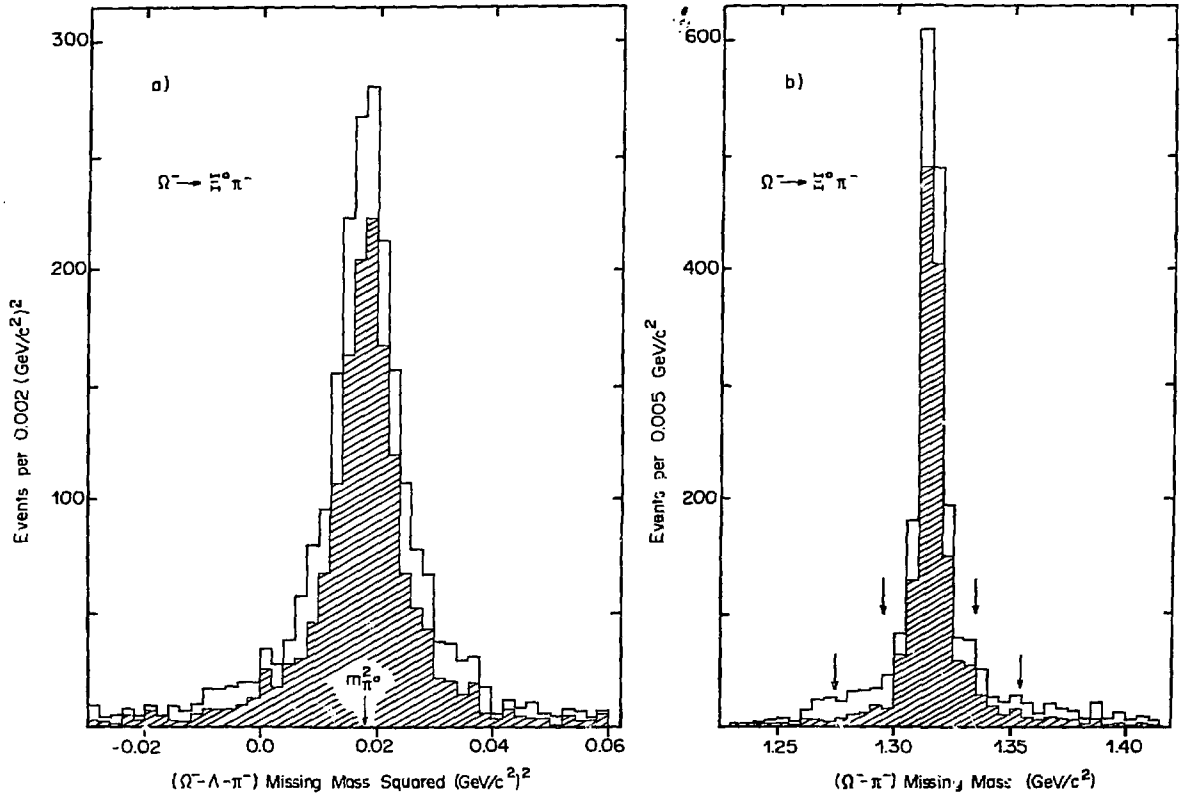
a)
$\Omega^- \to \Lambda\pi^0\pi^-$
$m^2_{\pi^0}$
Events per 0.002 $(GeV/c^2)^2$
$(\Omega^- - \Lambda - \pi^-)$ Missing Mass Squared $(GeV/c^2)^2$
300
200
100
-0.02
0.0
0.02
0.04
0.06
b)
$\Omega^- \to \Lambda\pi^0\pi^-$
Events per 0.005 GeV/c^2
$(\Omega^- - \pi^-)$ Missing Mass (GeV/c^2)
600
400
200
1.25
1.30
1.35
1.40

Figure 10

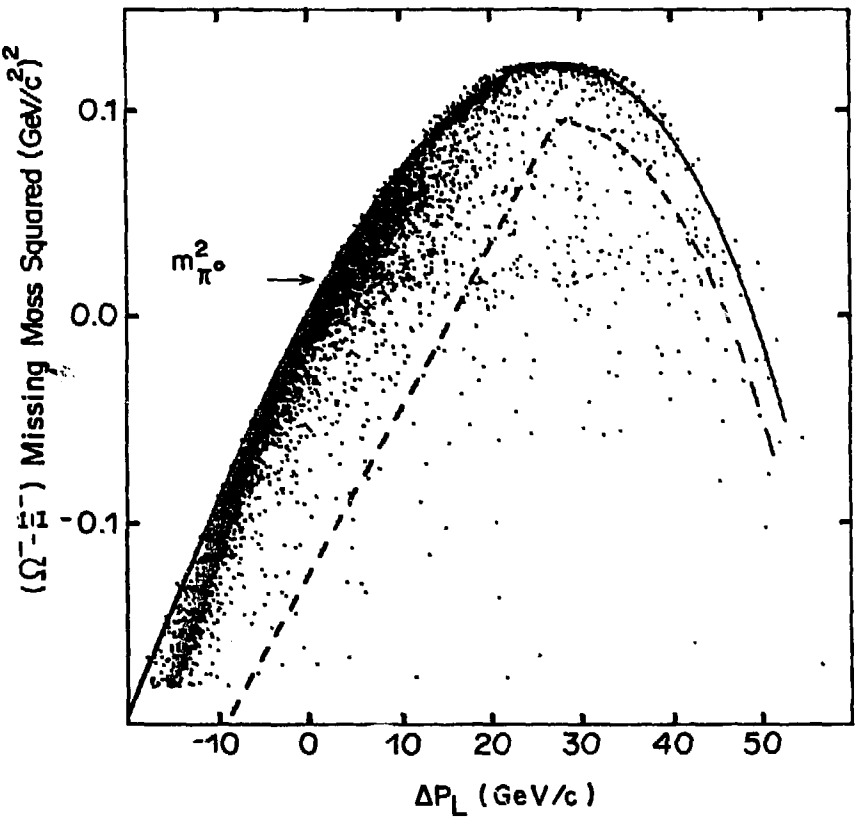
0.1
0.0
-0.1
$m^2_{\pi^0}$
$(\Omega^- - \Xi^-)$ Missing Mass Squared $(GeV/c^2)^2$
-10
0
10
20
30
40
50
ΔP_L (GeV/c)

Figure 11

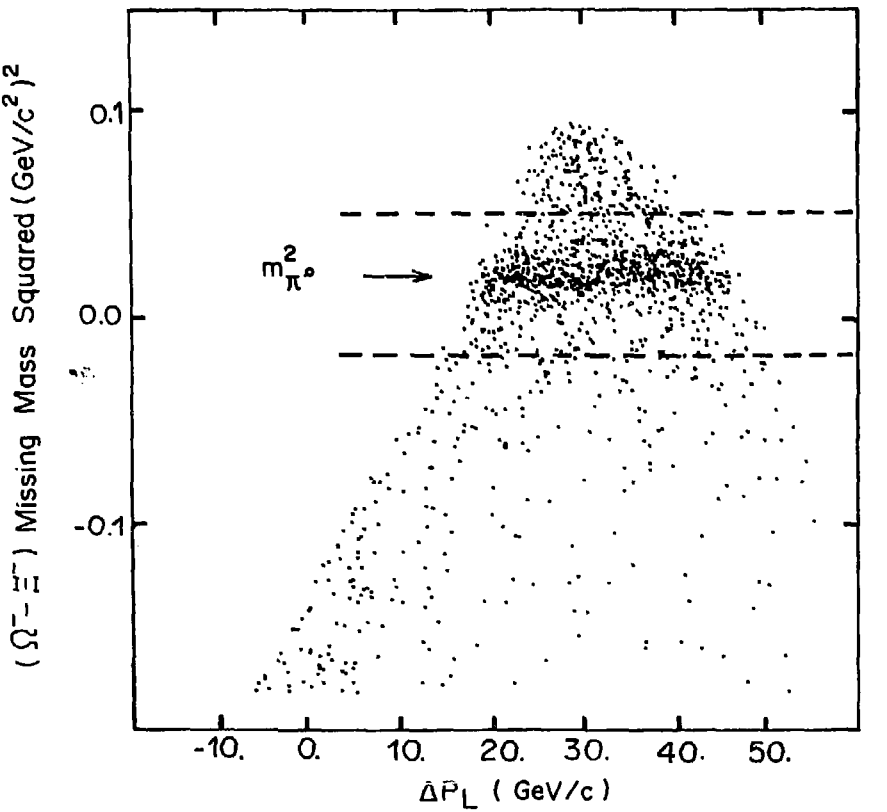
$(\Omega^- - \Xi^-)$ Missing Mass Squared $(GeV/c^2)^2$
0.1
0.0
-0.1
$m^2_{\pi^0}$
-10.
0.
10.
20.
30.
40.
50.
ΔP_L (GeV/c)

Figure 12

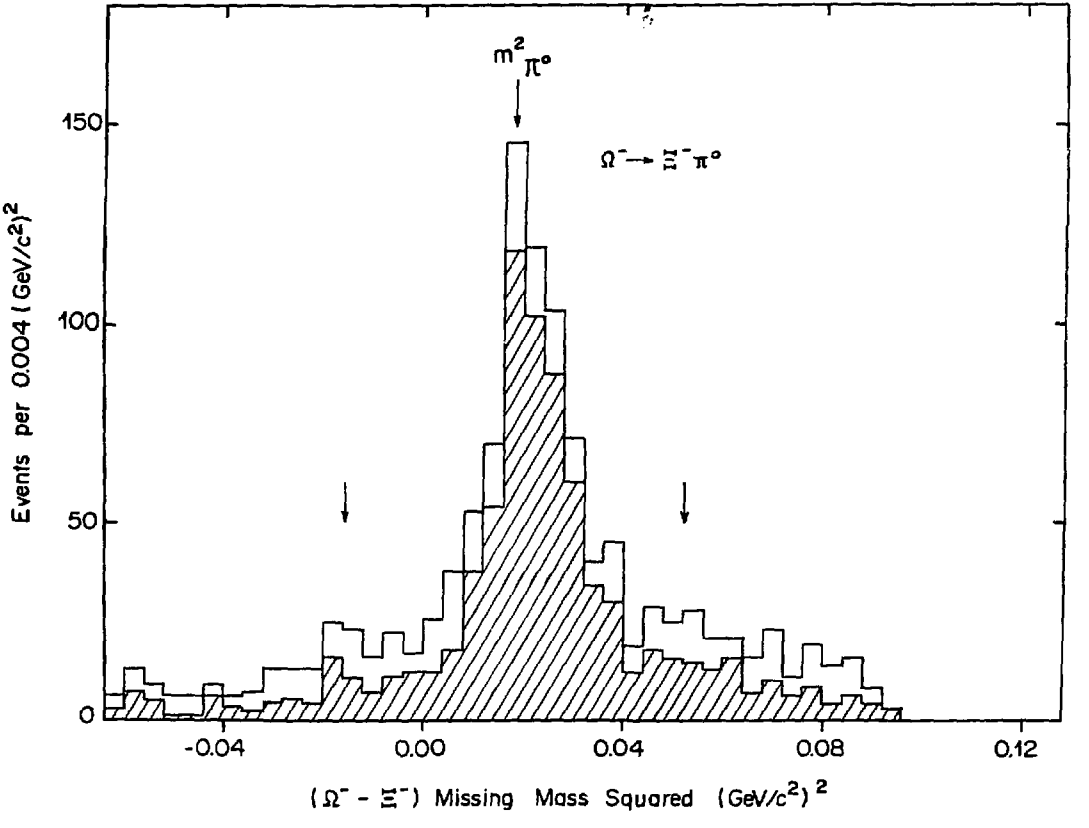
$m^2_{\pi^0}$
$\Omega^- \rightarrow \Xi^- \pi^0$
150
100
50
0
Events per 0.004 (GeV/c²)²
-0.04
0.00
0.04
0.08
0.12
$(\Omega^- - \Xi^-)$ Missing Mass Squared $(GeV/c^2)^2$

Figure 13

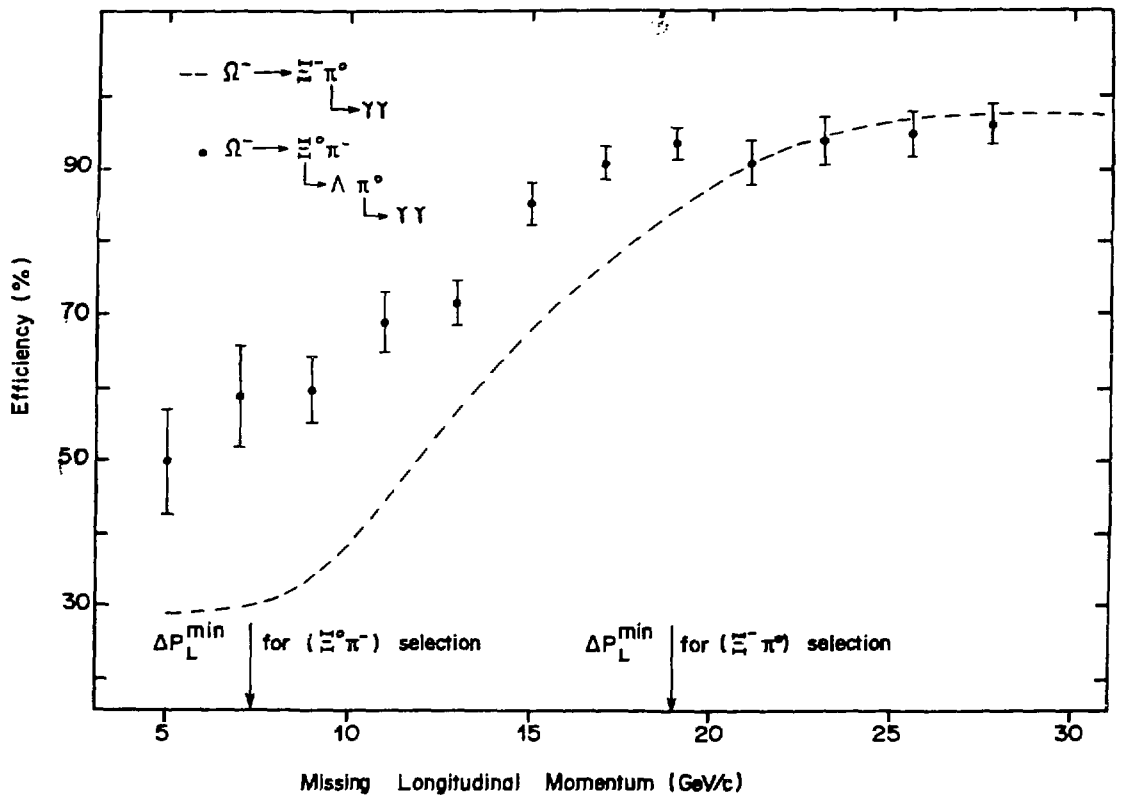
-- $\Omega^- \to \Xi^-\pi^0$
$\to \gamma\gamma$
• $\Omega^- \to \Xi^0\pi^-$
$\to \Lambda\,\pi^0$
$\to \gamma\gamma$
Efficiency (%)
90
70
50
30
ΔP_L^{min} for ($\Xi^0\pi^-$) selection
ΔP_L^{min} for ($\Xi^-\pi^0$) selection
5
10
15
20
25
30
Missing Longitudinal Momentum (GeV/c)

Figure 14

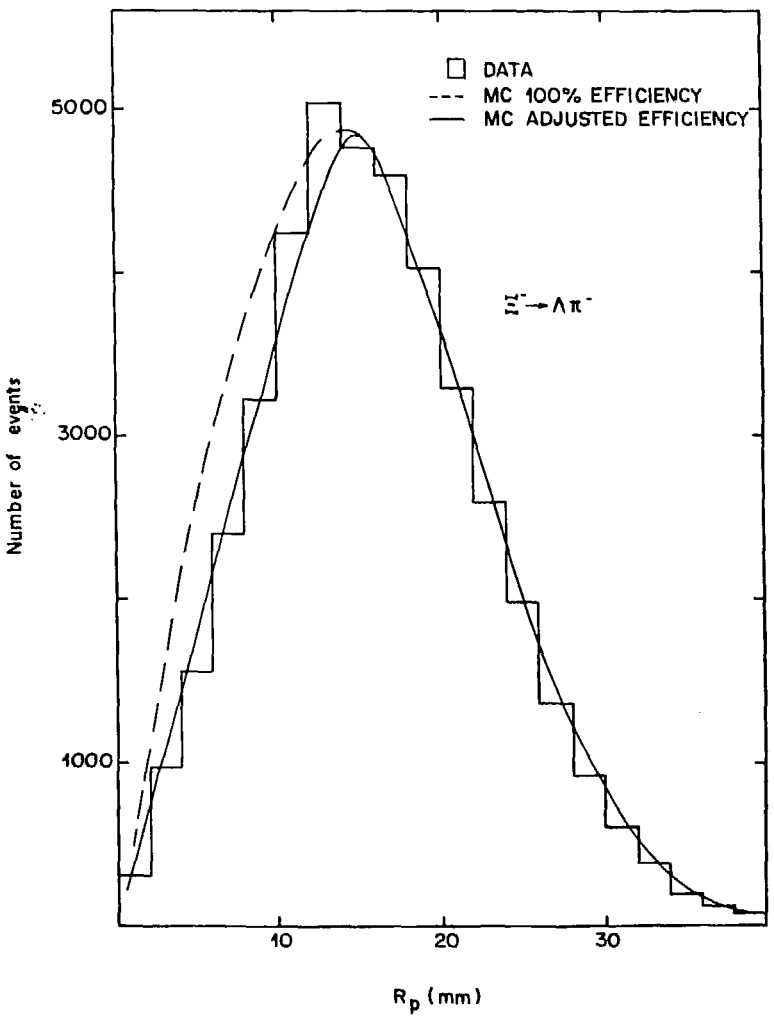
DATA
MC 100% EFFICIENCY
MC ADJUSTED EFFICIENCY
$\Xi^- \rightarrow \Lambda\pi^-$
Number of events
5000
3000
1000
10
20
30
R_p (mm)

Figure 15

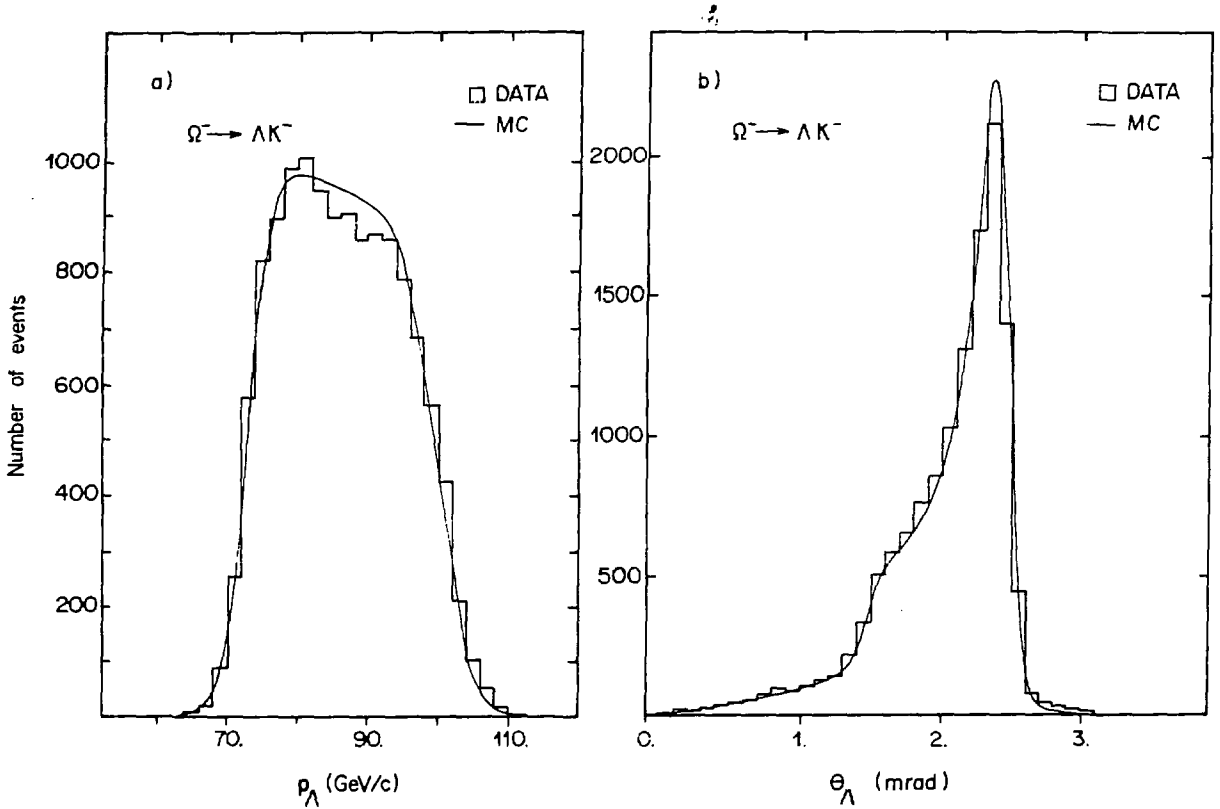
a)
□ DATA
— MC
Ω⁻ → ΛK⁻
Number of events
1000
800
600
400
200
70.
90.
110.
p_Λ (GeV/c)
b)
□ DATA
— MC
Ω⁻ → ΛK⁻
2000
1500
1000
500
0.
1.
2.
3.
θ_Λ (mrad)

Figure 16

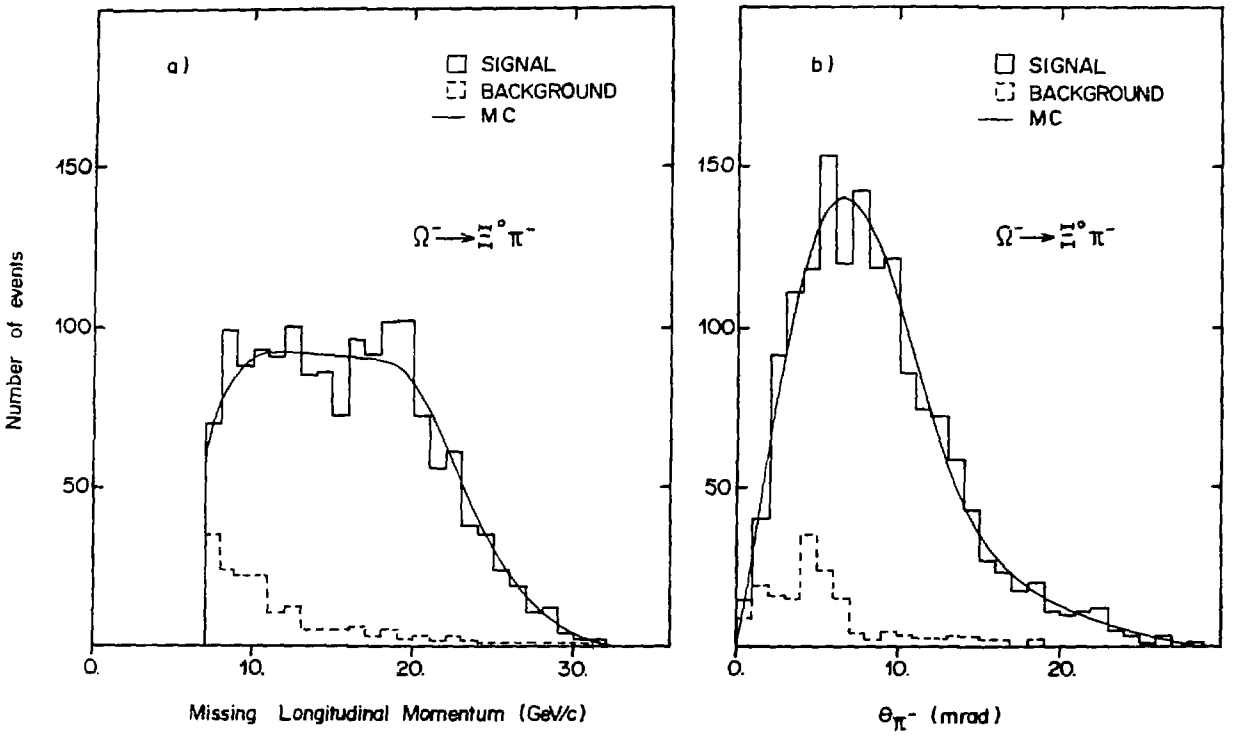
a)
SIGNAL
BACKGROUND
MC
$\Omega^- \rightarrow \Xi^0 \pi^-$
150
100
50
0.
10.
20.
30.
Number of events
Missing Longitudinal Momentum (GeV/c)
b)
SIGNAL
BACKGROUND
MC
$\Omega^- \rightarrow \Xi^0 \pi^-$
150
100
50
0.
10.
20.
θ_{π^-} (mrad)

Figure 17

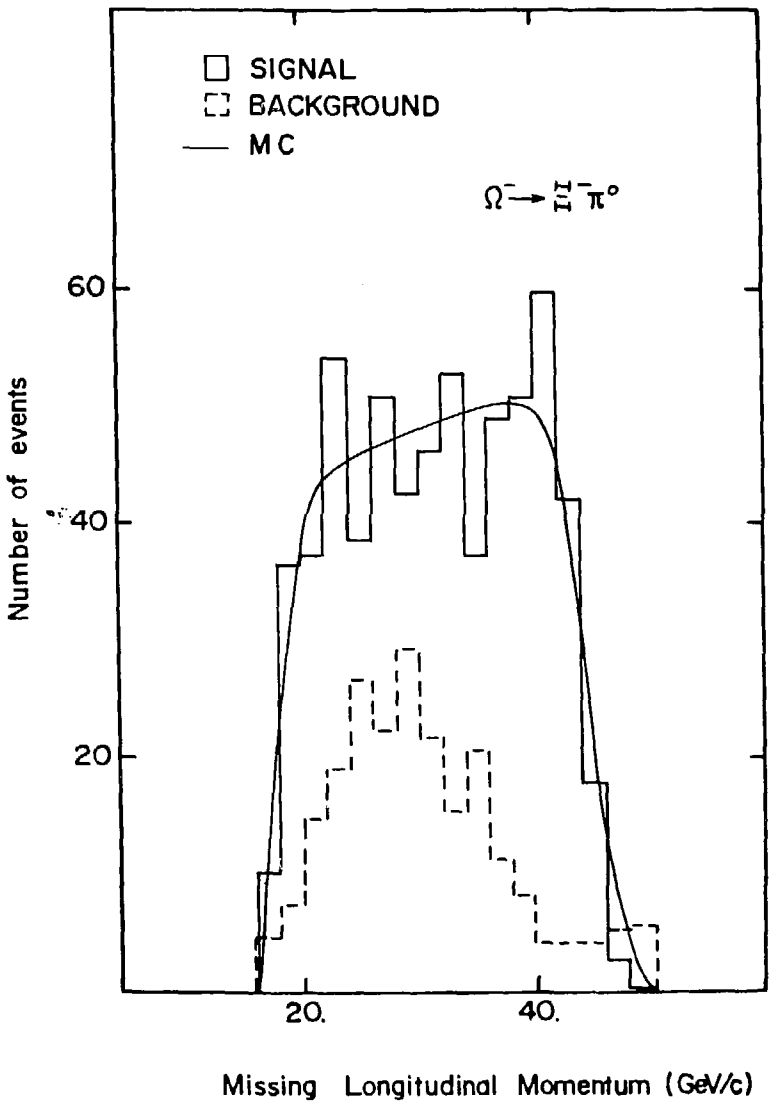
SIGNAL
BACKGROUND
MC
$\Omega^- \rightarrow \Xi^- \pi^\circ$
60
40
20
Number of events
20.
40.
Missing Longitudinal Momentum (GeV/c)

Figure 18

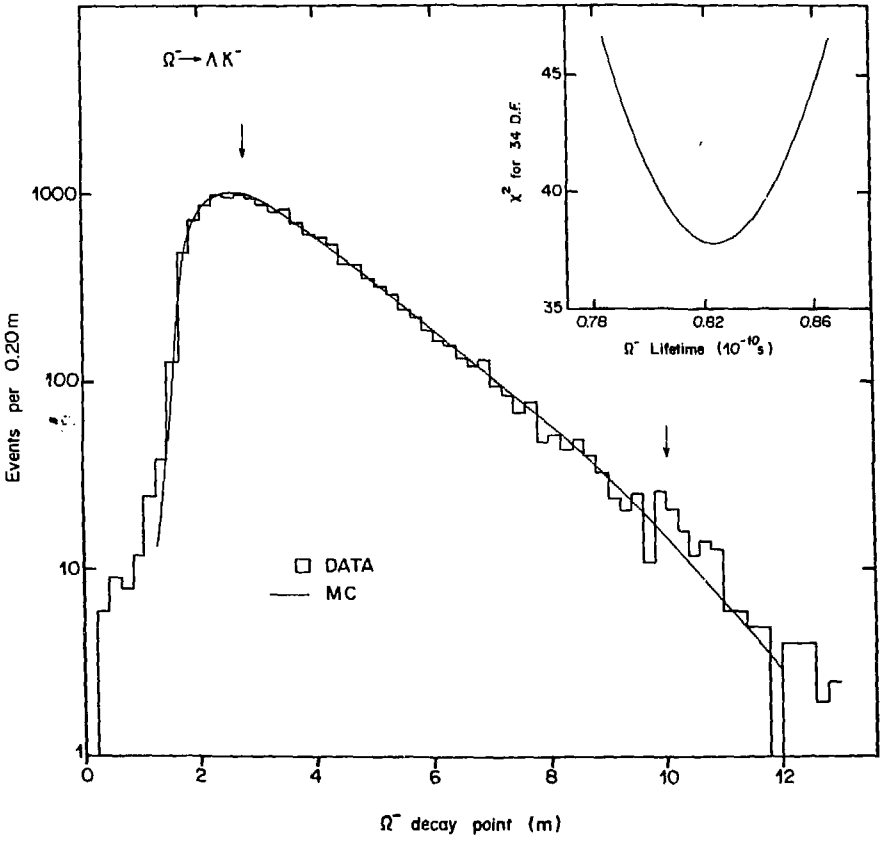
Ω⁻→ΛK⁻
Events per 0.20 m
1000
100
10
1
0
2
4
6
8
10
12
Ω⁻ decay point (m)
DATA
MC
χ² for 34 D.F.
45
40
35
0.78
0.82
0.86
Ω⁻ Lifetime (10⁻¹⁰s)

Figure 19

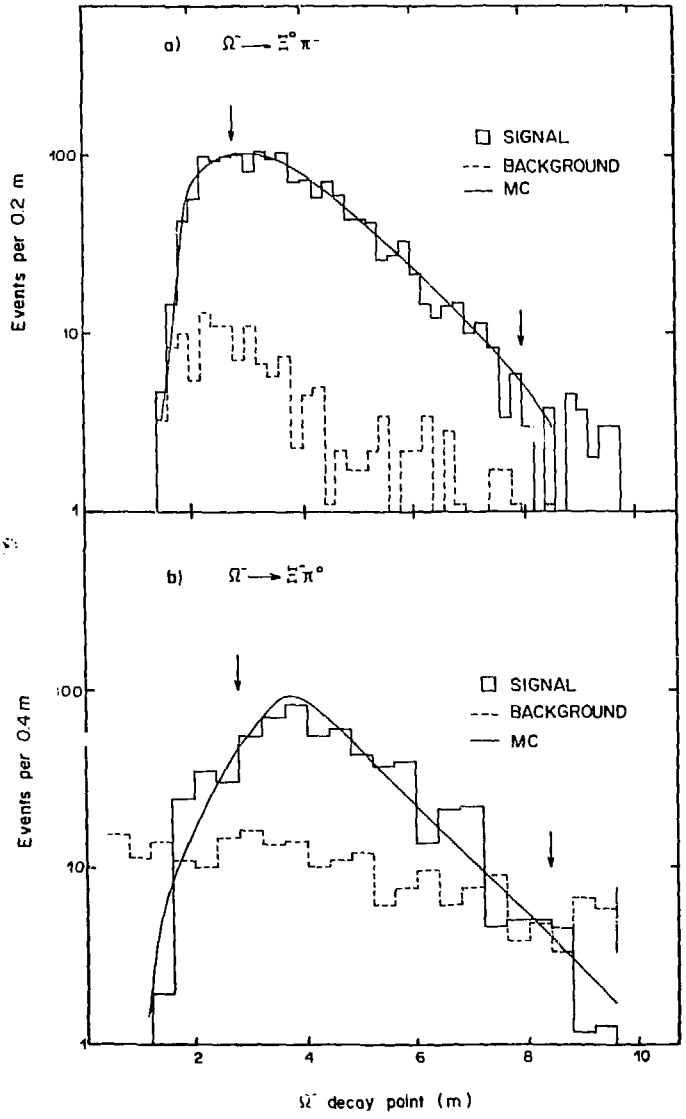
a) $\Omega^- \rightarrow \Xi^0\pi^-$
SIGNAL
BACKGROUND
MC
Events per 0.2 m
100
10
1
b) $\Omega^- \rightarrow \Xi^-\pi^0$
SIGNAL
BACKGROUND
MC
Events per 0.4 m
100
10
1
2
4
6
8
10
Ω^- decay point (m)

Figure 20

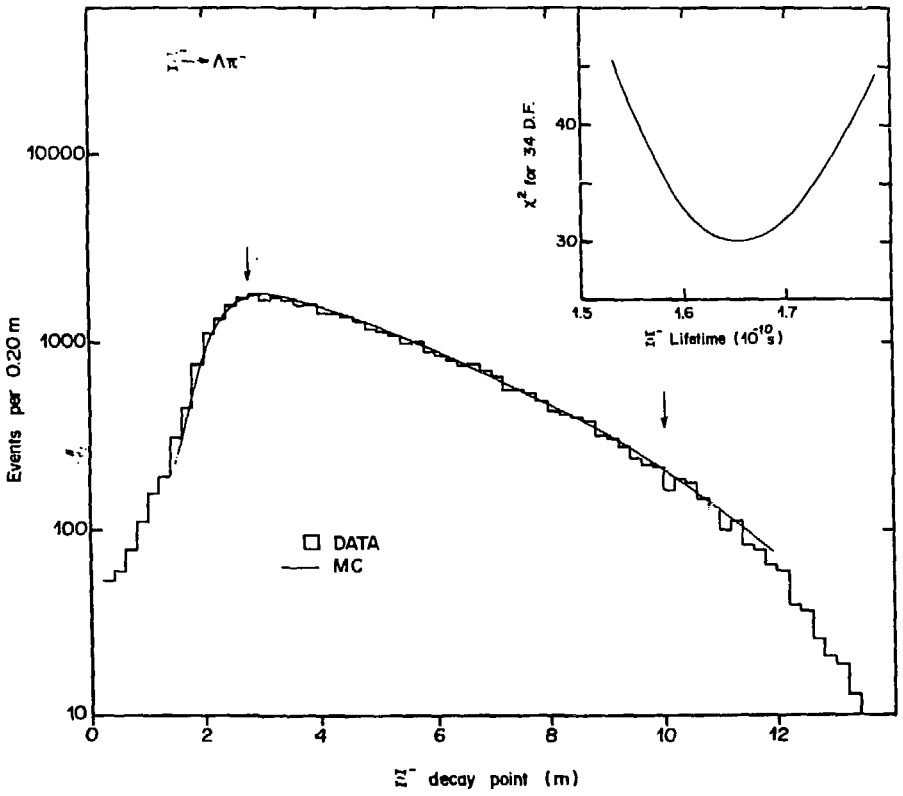
$\Xi^- \to \Lambda\pi^-$
10000
1000
100
10
Events per 0.20 m
0
2
4
6
8
10
12
Ξ^- decay point (m)
DATA
MC
40
30
χ^2 for 34 D.F.
1.5
1.6
1.7
Ξ^- Lifetime (10^{-10} s)

Figure 21

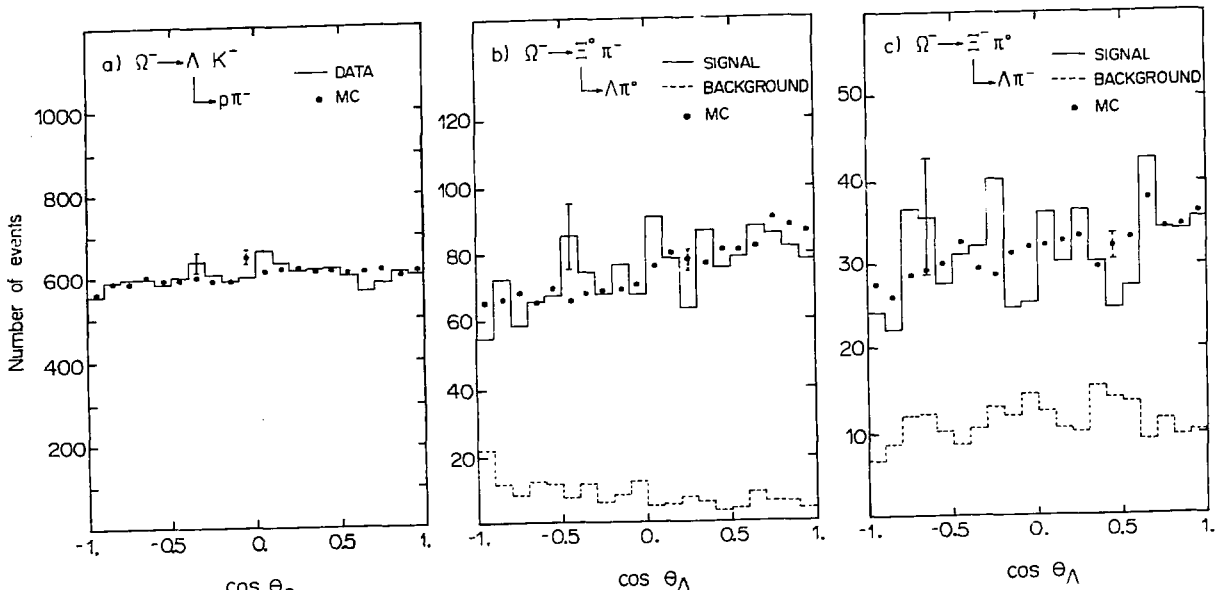
a) Ω⁻ → Λ K⁻
→ pπ⁻
DATA
MC
b) Ω⁻ → Ξ° π⁻
→ Λπ°
SIGNAL
BACKGROUND
MC
c) Ω⁻ → Ξ⁻ π°
→ Λπ⁻
SIGNAL
BACKGROUND
MC
Number of events
cos θp
cos θΛ
cos θΛ

Figure 22

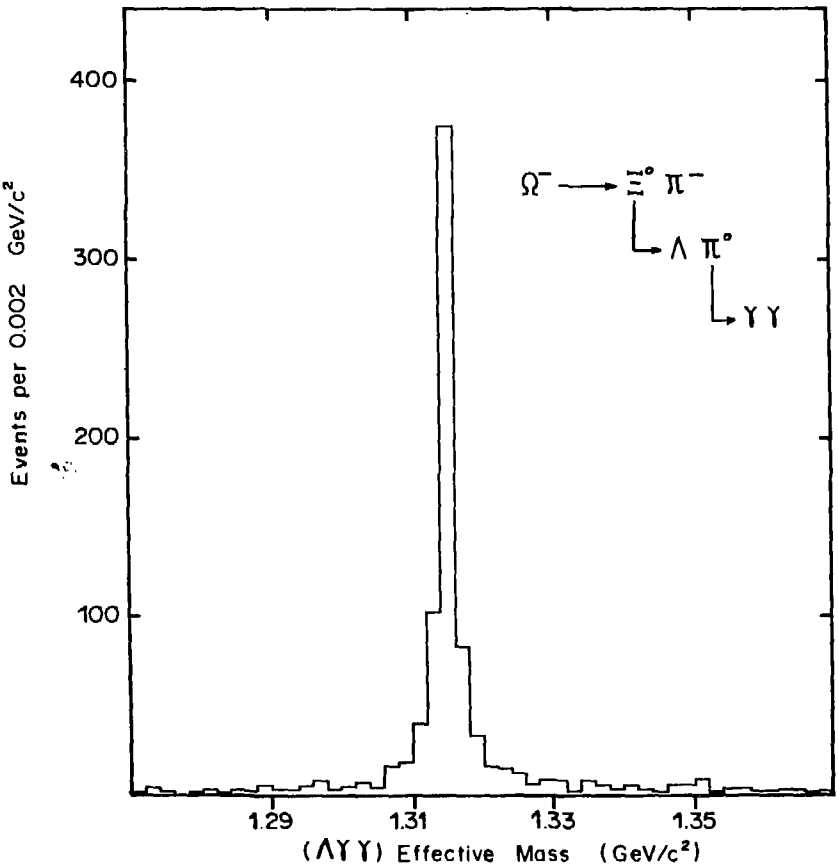
400
300
200
100
Events per 0.002 GeV/c²
Ω⁻ → Ξ⁰ π⁻
Λ π⁰
γ γ
1.29
1.31
1.33
1.35
(Λγγ) Effective Mass (GeV/c²)

Figure 23

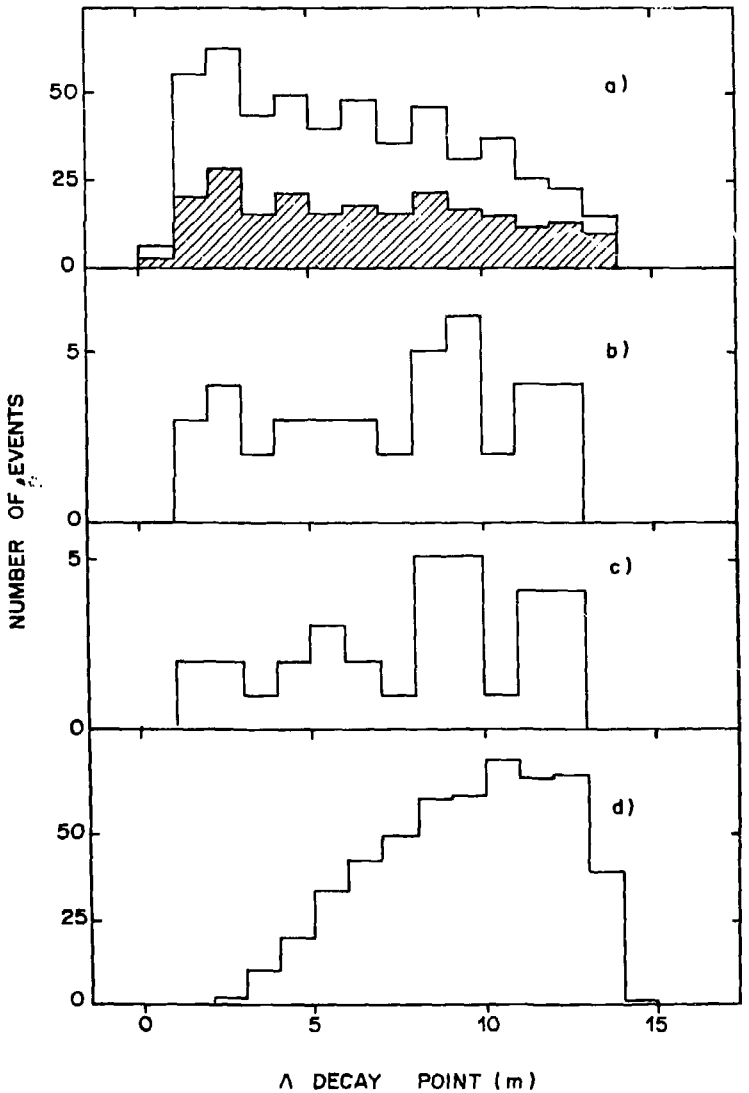
a)
b)
c)
d)
50
25
0
5
0
5
0
50
25
0
0
5
10
15
NUMBER OF Λ EVENTS
Λ DECAY POINT (m)

Figure 24

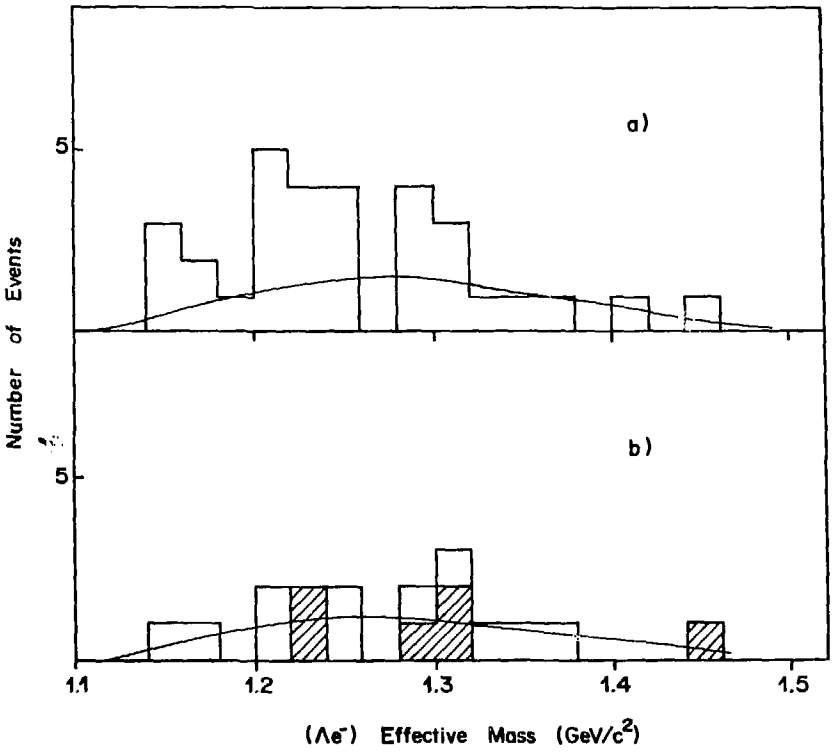

Figure 25

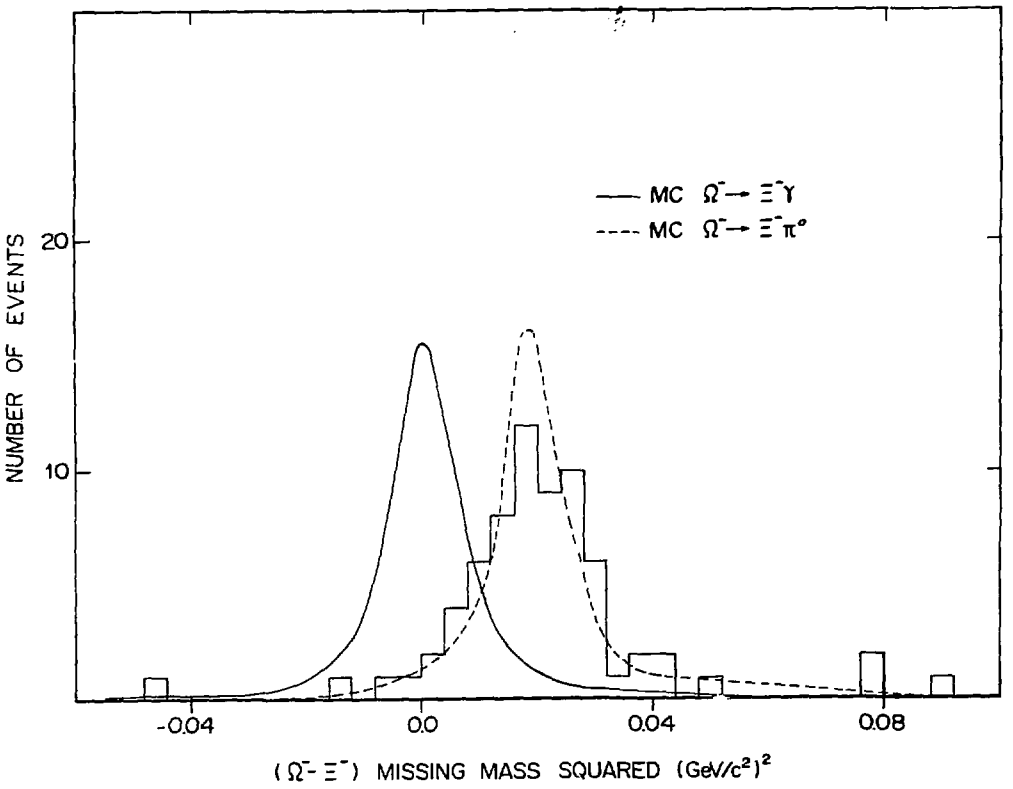
MC Ω⁻→ Ξ⁻γ
MC Ω⁻→ Ξ⁻π°
NUMBER OF EVENTS
20
10
-0.04
0.0
0.04
0.08
(Ω⁻- Ξ⁻) MISSING MASS SQUARED (GeV/c²)²

Figure 26

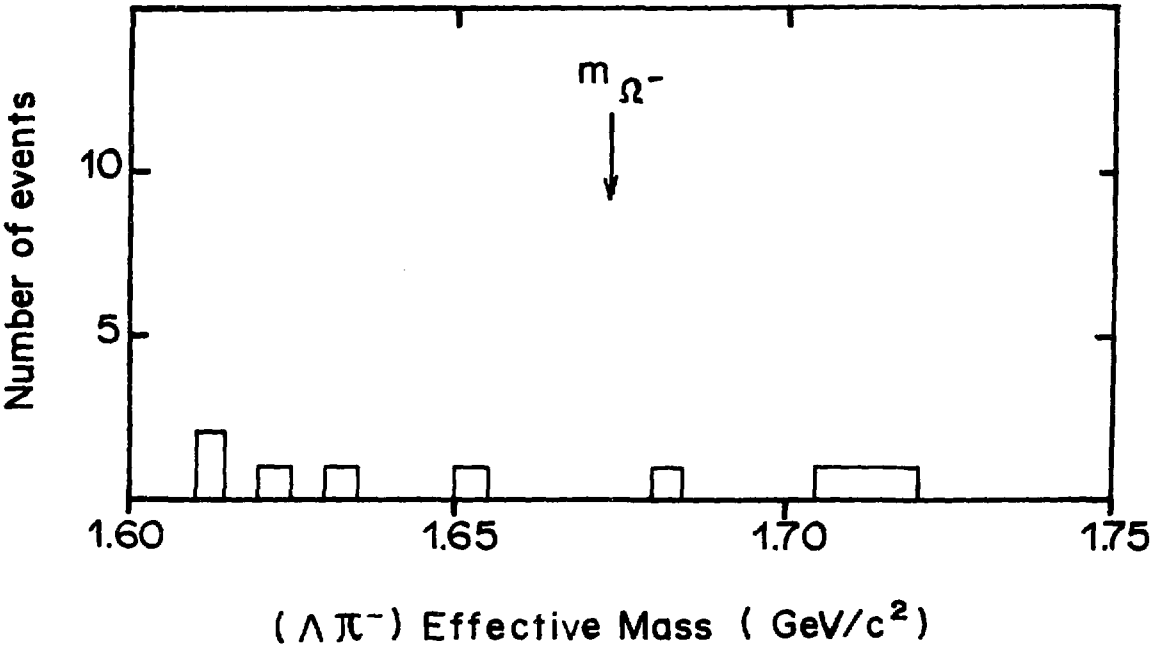
Number of events
10
5
m_{Ω^-}
1.60
1.65
1.70
1.75
$(\Lambda\pi^-)$ Effective Mass (GeV/c^2)

Figure 27

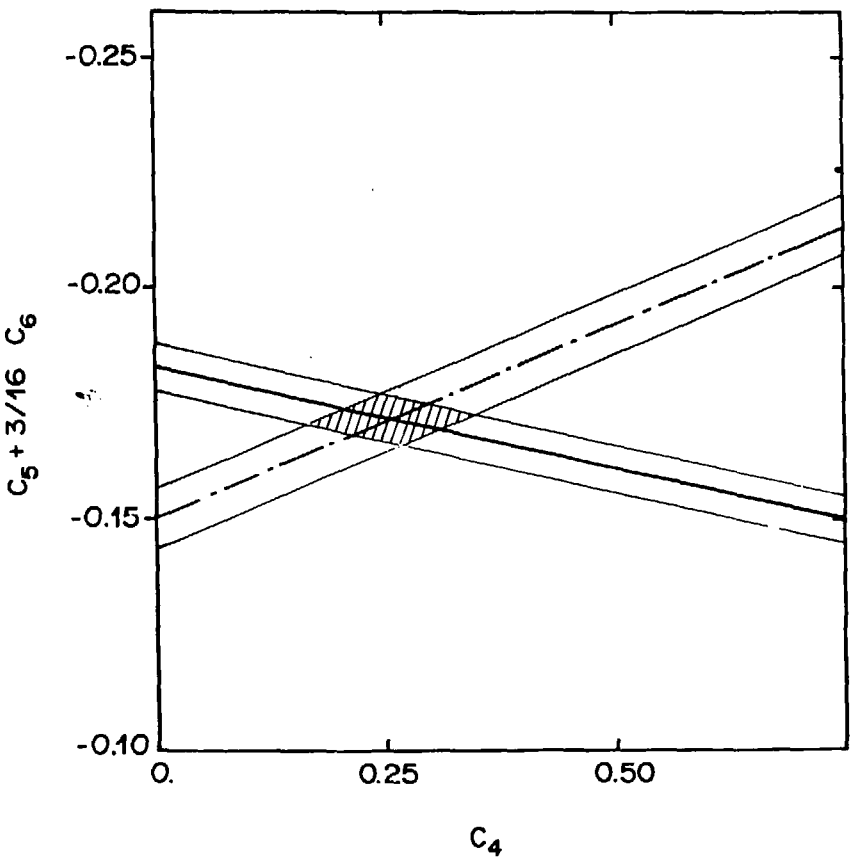

Figure 28

Imprimé
au Centre de
Recherches Nucléaires
Strasbourg
1984